AGU ADVANCING EARTH AND SPACE SCIENCES

JGR Planets

RESEARCH ARTICLE

10.1029/2026JE009660

Key Points:

- An Australian vertisol overlying a magnecrete horizon hosts multi-generational Mg-carbonate nodules
- Magnecrete genesis and alteration records a near-surface interplay of hydrologic and sedimentary processes relevant for Mars and its past
- Evidence suggests magnesite forms via pedogenic and diagenetic processes from percolating meteoric water and groundwater capillary action

Supporting Information:

Supporting Information may be found in the online version of this article.

Correspondence to:

E. L. Cardarelli,
ecardare@epss.ucla.edu

Citation:

Cardarelli, E. L., Present, T. M., Vasconcelos, P. M., Kah, L. C., Swindle, C., Bhattacharjee, S., & Farley, K. (2026). Formation and alteration of magnesite nodules from Kunwarara, Queensland, Australia, as an analog to Mg-carbonate formation on Mars. *Journal of Geophysical Research: Planets*, *131*, e2026JE009660. https://doi.org/10.1029/2026JE009660

Received 9 JAN 2026
Accepted 11 AUG 2026

Author Contributions:

Conceptualization: E. L. Cardarelli, T. M. Present, P. M. Vasconcelos, C. Swindle, S. Bhattacharjee, K. Farley
Data curation: E. L. Cardarelli, T. M. Present
Formal analysis: E. L. Cardarelli, T. M. Present, L. C. Kah
Funding acquisition: T. M. Present, P. M. Vasconcelos, K. Farley
Investigation: E. L. Cardarelli, T. M. Present, P. M. Vasconcelos, L. C. Kah, S. Bhattacharjee

Formation and Alteration of Magnesite Nodules From Kunwarara, Queensland, Australia, as an Analog to Mg-Carbonate Formation on Mars

E. L. Cardarelli[1,2], T. M. Present[3], P. M. Vasconcelos[4], L. C. Kah[5], C. Swindle[3,6], S. Bhattacharjee[3], and K. Farley[3]

[1]Department of Earth, Planetary, and Space Sciences, University of California, Los Angeles, CA, USA, [2]Jet Propulsion Laboratory, California Institute of Technology, Pasadena, CA, USA, [3]Division of Geologic and Planetary Sciences, California Institute of Technology, Pasadena, CA, USA, [4]The University of Queensland, Brisbane, QLD, Australia, [5]Department of Earth, Environmental and Planetary Sciences, University of Tennessee, Knoxville, TN, USA, [6]Department of Materials Science and Engineering, University of California, Los Angeles, CA, USA

Abstract Magnesite ($MgCO_3$) is a magnesium (Mg) carbonate mineral that records the aqueous environmental conditions of its formation. On Earth, magnesite forms in metamorphic, diagenetic or pedogenic environments, and distinguishing between these environments is critical for understanding the fluid chemistry during magnesite precipitation. Mg carbonates have been observed across the Nili Fossae region on Mars and in Jezero crater by orbital spectroscopy as well as in situ by the Perseverance rover. Rover acquired core samples with Mg carbonates may provide constraints on the chemical conditions of the ancient aqueous environments of Jezero crater, and may also be an important target for the preservation of potential biosignatures. This work explores magnesite phases found in Vertisols of the Kunwarara Mine, Australia, as a potential analog environment for magnesite on Mars. We document the principal microtextures, mineralogical context, and elemental compositions. We investigate the processes involved in the formation and diagenesis of magnesite nodules and a magnecrete. Kunwarara hosted magnesite shows complex textural relationships at the outcrop scale, and these relationships extend down to the nanoscale in samples that were collected along a depth profile. By characterizing textural and chemical variations in magnesite at different scales, this work reveals a continuum between diagenetic and pedogenic magnesites. It illustrates that diagenetic reactions produce magnesite from ascending Mg^{2+}-rich groundwater interacting with detrital phases; groundwater interaction with descending meteoric solutions result in the conversion of magnesite into authigenic dolomite. Overall, this work shows how the superposition of textures and elemental compositions permits reconstruction of pedogenic processes leading to magnesite authigenesis.

Plain Language Summary Magnesite ($MgCO_3$) is an important yet understudied carbon-storing mineral on Earth. It has been detected on Mars in ancient weathering profiles and within Jezero crater using orbital spectroscopy and instruments aboard the Perseverance rover. By studying magnesite occurrences on Earth, we can obtain valuable information about the chemical changes that might have occurred in the past environments of Jezero crater or other localities on Mars. Critically, magnesite is a phase that forms under habitable conditions from water and carbon, potentially preserving evidence of ancient extraterrestrial life. To this end, magnesite at Jezero crater has been sampled for potential return to Earth. This study investigates magnesites and sediments from the Kunwarara deposit in Australia in a vertical weathered soil profile that may be relevant to Mg-carbonates on Mars. Small-scale features of magnesite are examined here, with a particular focus on how magnesite precipitates and changes over time. The mineral-based work shows that primary magnesite can transform into other mineral phases, such as dolomite, through interactions with surficial waters. By studying the textures and chemical composition of magnesite samples on Earth, scientists can better understand the processes that led to the formation of magnesite on Mars.

1. Introduction

The formation of magnesium (Mg) carbonate minerals is one mechanism which links both the carbon and water cycles. Mg-carbonate phases include amorphous magnesium carbonate, dolomite ($CaMg(CO_3)_2$, magnesite ($MgCO_3$), and various hydrous carbonates such as nesquehonite ($MgCO_3{\cdot}3H_2O$) and hydromagnesite ($Mg_5(CO_3)_4(OH)_2{\cdot}4H_2O$). On Earth, Mg-carbonate phases form in a variety of settings, including as an alteration

Methodology: E. L. Cardarelli, T. M. Present, C. Swindle, S. Bhattacharjee
Project administration: T. M. Present, P. M. Vasconcelos, K. Farley
Resources: E. L. Cardarelli, T. M. Present, P. M. Vasconcelos, L. C. Kah
Software: E. L. Cardarelli
Supervision: T. M. Present, P. M. Vasconcelos, K. Farley
Validation: E. L. Cardarelli, T. M. Present
Visualization: E. L. Cardarelli, T. M. Present, L. C. Kah, S. Bhattacharjee
Writing – original draft: E. L. Cardarelli, T. M. Present, L. C. Kah
Writing – review & editing: E. L. Cardarelli, T. M. Present, P. M. Vasconcelos, L. C. Kah, C. Swindle, K. Farley

phase within ultramafic complexes, as a primary pedogenic phase within soils, as a diagenetic phase within soils and playas, and as a primary chemical precipitate within Mg-rich lakes and hydrothermal solutions (Pohl, 1989; Scheller et al., 2021). They have been studied in ultramafic (Falk & Kelemen, 2015; García Del Real & Vishal, 2016; Swindle, Vasconcelos, Dimarco, et al., 2025, Swindle, Vasconcelos, Dalleska, et al., 2025), lacustrine (Braithwaite & Zedef, 1996; Raudsepp et al., 2024; Valdespino-Castillo et al., 2022), marine (Lumsden, 1988), and playa environments (Mavromatis et al., 2021; Power et al., 2019). Outside Earth, Mg-carbonate phases have also been detected within martian meteorites such as ALH84001 (Mittlefehldt, 1994; Steele et al., 2022) and observed on Mars by orbital spectroscopy (Ehlmann et al., 2008; Horgan et al., 2020) as well as by in situ rover observations (Broz et al., 2024; Kalucha et al., 2024; Scheller et al., 2022; Williford et al., 2025). The occurrences of Mg-carbonate phases on Mars are thought to have been formed primarily in subsurface diagenetic settings (Scheller et al., 2021), which have fewer terrestrial analogs. However, the key controls on magnesite formation, such as the pressure/temperature conditions, relative time of formation, and effects of burial diagenesis—all remain poorly constrained.

On Earth, carbonate minerals which form at the interface between the hydrosphere, biosphere, atmosphere, and solid Earth are typically calcium (Ca) rich (Alonso-Zarza & Wright, 2010; Bachman & Machette, 1977; Goudie, 1983) and accumulate through time in pedogenic environments as calcretes. Magnesite, although less common, often occurs as weathering products of ultramafic rocks through low-temperature processes in semi-arid to arid environments (Oskierski et al., 2019; Power et al., 2019) and has a higher predicted solubility than Ca-carbonates (Catling, 1999). The relative paucity of Mg-carbonates compared to Ca-carbonates reflects Ca enrichment in Earth's continental crust; in contrast, weathering of Ca-poor ultramafic protoliths, such as those that are more common on Mars, preferentially generates Mg-carbonates.

Terrestrial calcrete forms in two primary ways. Pedogenic calcrete forms where Ca-rich waters infiltrate into soil horizons, precipitating carbonate minerals along the infiltration pathway (Alonso-Zarza & Wright, 2010). Groundwater calcrete, in turn, forms when Ca-rich waters ascend from the groundwater table through evapotranspiration and capillary action, forming extensive carbonate cement horizons with nodular facies toward the top of the profile (Alonso-Zarza, 2003). Previous studies have documented pedogenic and diagenetic dolomites and magnesites in ultramafic magmatic rocks, sabkhas, playas, lacustrine environments, palustrine environments, volcanic tephras, and forest soils where redox shifts occur (Diaz-Hernandez et al., 2018; Fischel et al., 2023; Pohl, 1989; Riechelmann et al., 2020; Zamanian et al., 2016).

This work examines Mg-carbonate-bearing rocks and soils of the Kunwarara area of central Queensland, Australia. Here, late Precambrian serpentinite and diverse Phanerozoic crustal igneous, metamorphic, and sedimentary rocks surround a hydrologic catchment that has been filled by late Cenozoic fluvial sediments. These sediments have developed into Mg-carbonate-bearing Vertisol profiles resulting from pedogenic alteration over prolonged periods of time (Lin, 2011; Milburn & Wilcock, 1998; Swindle, Vasconcelos, Dimarco, et al., 2025, Swindle, Vasconcelos, Dalleska, et al., 2025). Mg-carbonates within these materials are hypothesized to be derived via a combination of pedogenic (i.e., authigenic reactions occurring in the soil) precipitation and secondary alteration processes. Neoformed magnesite occurs as both discrete nodules within arkosic sand and expandable clay, and as extensive stratiform bodies, similar to those observed at the nearby Yaamba Mine (Swindle, Vasconcelos, Dimarco, et al., 2025, Swindle, Vasconcelos, Dalleska, et al., 2025). These occurrences provide an ideal opportunity to trace the physicochemical processes leading to the precipitation of magnesium carbonates from low-temperature Mg-bearing solutions coupled to subsequent groundwater alteration and evolution of the substrate. By identifying microscale textural and chemical variation within the magnesites of Kunwarara, this work documents the occurrence of multiple magnesite types that are useful analogs for understanding the genesis of Mg-carbonates detected at Jezero crater and more broadly in weathering sequences on Mars.

Here, we use a suite of integrated analytical techniques, including scanning electron microscopy (SEM) with energy dispersive spectroscopy (EDS), X-ray fluorescence mapping (XRF), and X-ray diffraction (XRD) analyses, to define the mineralogical and chemical variation of the magnesite and associated sediment collected across the Kunwarara weathering horizons. By leveraging measurements from the outcrop (meter-scale) to nanometer-scale, this work identifies and characterizes textural and chemical variation in the magnesite and other pedogenic minerals to reconstruct the genesis and evolution of these complex Mg-carbonate bearing assemblages.

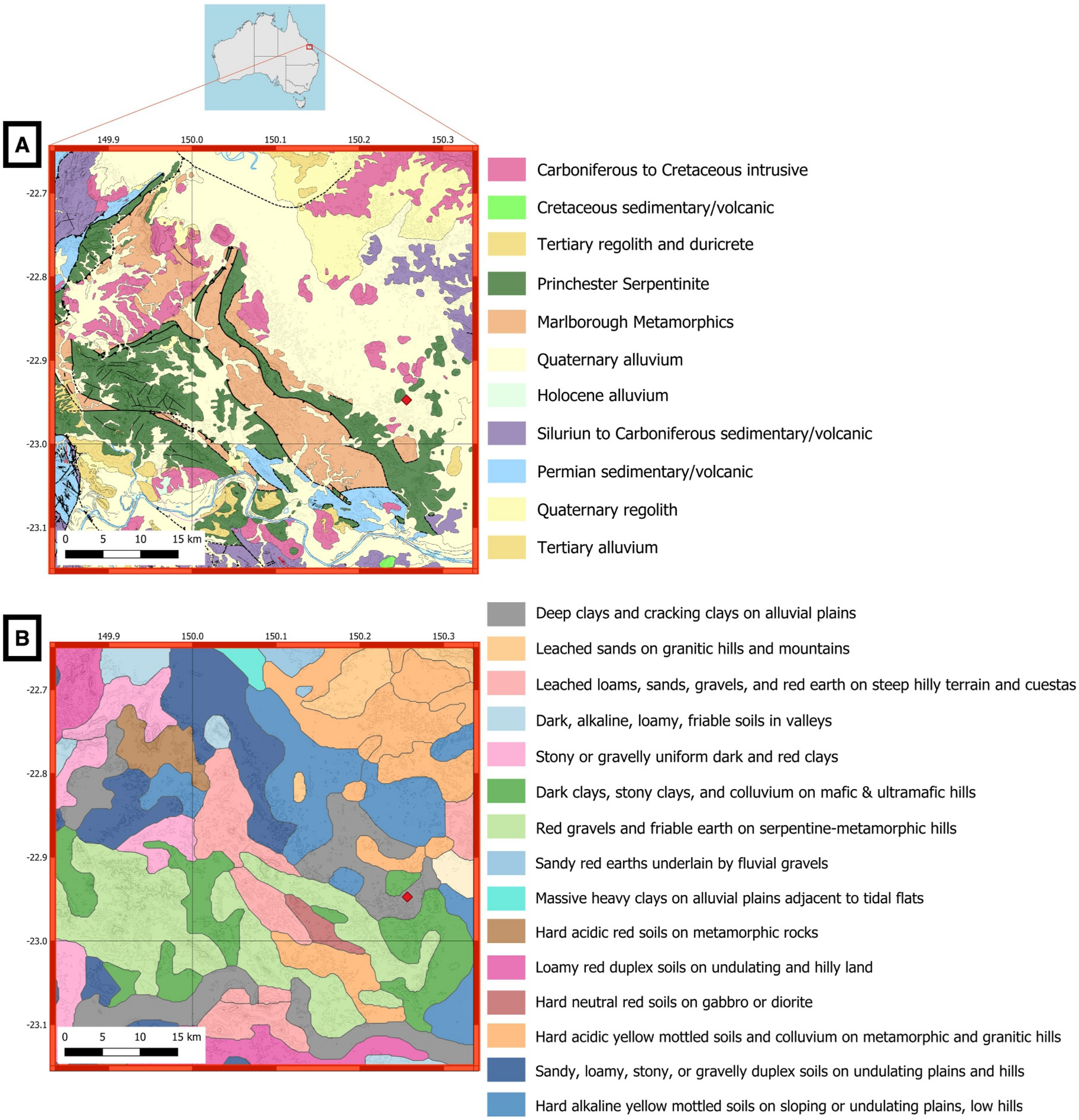

Figure 1. Geologic and pedogenic context of Kunwarara, Queensland, Australia. Modified from the GSQ 2012 geologic map, ASTER GDEM v3, and CSIRO Digital Atlas of Australian Soils. (a) The geologic context of Kunwarara, Queensland, Australia is presented at the regional scale and within the broader box of the broader Australia context inset map in red. For both panels, the locality sampled is denoted with a red diamond and located on Quaternary alluvium, surrounded by the Princhester Serpentinite. (b) The pedologic context of greater Kunwarara area (i.e., the same area as presented in (a) is shown with the soil units labeled). The pedologic unit hosting the magnesite and sediment matrix investigated in this work is indicated in dark gray, as deep clays and cracking clays on alluvial plains.

2. Materials and Methods

2.1. Geologic Setting

Magnesite occurs in both ultramafic and sedimentary rocks throughout the New England Fold Belt in eastern Australia (Oskierski et al., 2013, 2019; Swindle, Vasconcelos, Dimarco, et al., 2025, Swindle, Vasconcelos, Dalleska, et al., 2025). The Kunwarara quarries of central Queensland, Australia host some of the largest cryptocrystalline sedimentary magnesite deposits in the world (Milburn & Wilcock, 1998). This area is surrounded by the Princhester Serpentinite (Figure 1a), a deeply weathered ultramafic bedrock that is assumed to be the primary source of regional aqueous weathering products (McNeil & Raymond, 2013; Swindle, Vasconcelos, Dimarco, et al., 2025, Swindle, Vasconcelos, Dalleska, et al., 2025). The late Precambrian Princhester

Serpentinite complex was emplaced within the New England Fold Belt during the early-mid Paleozoic. The serpentinite was later intruded, metamorphosed, and deformed by the Permo-Triassic aged Hunter-Bowen Orogeny (Bruce & Niu, 2000; Evans & Roberts, 1979; Murray, 2007). Cenozoic weathering and erosion of the Queensland passive margin then led to deep, lateritic weathering of bedrock (Batianoff & Singh, 2001; Foster et al., 2002; Zeissink, 1969), followed by Neogene to recent sediment deposition and pedogenesis of fluvial-alluvial sedimentary strata under less intense arid to semi-arid weathering conditions (e.g., Vertisol-forming climates) (Batianoff & Singh, 2001; Forster & Baker, 1997). The field site (red diamond, Figure 1) hosts deep overlying clays on alluvial plains that experience seasonally wet conditions (dark gray unit, Figure 1b). These sedimentary units are represented by unlithified arkose, subarkose, and lithic arenite sands and mud capped by a smectitic Vertisol of variable thickness and composition. Below the smectitic soil, within the bedded sand, magnesite occurs as centimeter- to decimeter-scale nodules and meter-scale stratiform bodies near the modern watertable (Figures 2 and 3).

2.2. Sample Collection and Analysis

Samples were collected from a 12-m Vertisol (Figure 2) exposed at the edge of a magnesite mine pit within the Kunwarara Qmag magnesite mine (centered at 22°55′S, 150°13′E, Kunwarara, Queensland, Australia, Figure 1) in August 2019. At the field site (red diamond, Figure 1), dark clays were found above friable, nodular magnesite in the upper subsection (Figure 2a) and cemented magnesite in the lower subsection (Figure 2b). At the outcrop scale, six pedogenic horizons (K-3.4: 0–6.8 m depth belowground surface (bgs), K-7.6: 6.8–8.3 m bgs, K-8.8: 8.3–9.3 m bgs, K-9.8: 9.3–10.3 m bgs, K-10.8: 10.3–11.3 m bgs, K-11.8: 11.3–12.3 m bgs; Table S1 in Supporting Information S1) were identified and sampled. In each of these intervals, the host sediment as well as magnesite was sampled where present (Figure 2, Table S1 in Supporting Information S1). Magnesite was not found in the surface horizon (K-3.4) and host sediment was not retrieved from the deepest exposed horizon (K-11.8). Magnesite nodule samples were photographed at the Jet Propulsion Laboratory (JPL) and thin-sectioned (24 × 46 mm dimensions) by Wagner Petrographic for microscopy.

XRD of both the magnesite and host sediment samples provided the initial assessment of the mineralogy of the magnesite and host sediment compositions. Subsamples of the magnesite and the host sediment were air-dried and homogenized with a mortar and pestle prior to XRD. The magnesite samples from the section transect were characterized with the Rigaku SmartLab XRD instrument in the California Institute of Technology Beckman Institute X-Ray Powder Crystallography Facility. In addition, sediment samples from the following horizons (K-3.4, K-7.6, K-8.8, K-9.8, K-10.8) were characterized by K/T Geosciences, Gunnison, CO on a Siemens D500 automated powder diffractometer equipped with a copper X-ray source (40 kV, 30 mA) and a scintillation X-ray detector. For bulk sediment XRD analysis, homogenized powder for each sample was dried, disaggregated, and then loaded into a metal sample holder to produce random bulk mounts. The bulk powder samples were analyzed over an angular range of 5°–6° 2θ at a scan rate of 1° per minute, producing the air-dried treatment results. The clay mounts were then exposed to ethylene glycol vapor for a minimum of 12 hr and then analyzed by XRD again to determine clay mineral swelling in the glycolated, oriented clay-fraction. The air-dried and glycolated XRD patterns for each sample were compared for clay mineral identifications, and used to produce semi-quantitative determinations of mineral proportions from the bulk analyses with Jade Software (Materials Data, Inc., Livermore, CA) and the Whole Pattern Fitting option.

Polished thin sections and freshly fractured sample chips were also used to characterize the fabric of the magnesite samples as well as the spatial distribution of mineralogical phases. Petrographic observations in plane and polarized light were conducted on polished thin sections at the California Institute of Technology on a Leica DM 2500 P microscope and at the University of Tennessee on an Olympus BX-60 microscope. Scanning electron microscopy with energy dispersive x-ray spectroscopy (EDS) measurements were completed in the JPL Astrobiogeochemistry Laboratory on polished thin sectioned magnesite samples and freshly fractured sample chips with a Hitachi SU 3500 VP-SEM under high vacuum mode with a dispersive spectroscopy system by Oxford Instruments X-MaxN for automated SEM/EDS elemental mapping and point analysis. SEM of the sediment material from the respective horizons sampled was completed in the Geological and Planetary Sciences (GPS) Analytical Facility at the California Institute of Technology with a Field Emission Scanning Electron Microscope (FE SEM) (Zeiss 1550 VP, operating in secondary electron and backscattered electron modes at 15 kV and 9 mm working distance on material pressed to carbon tape and coated with graphite. Elemental distributions were also mapped on the off-cut billets of the magnesite thin-sections in the Caltech GPS Analytical Facility using micro-X-

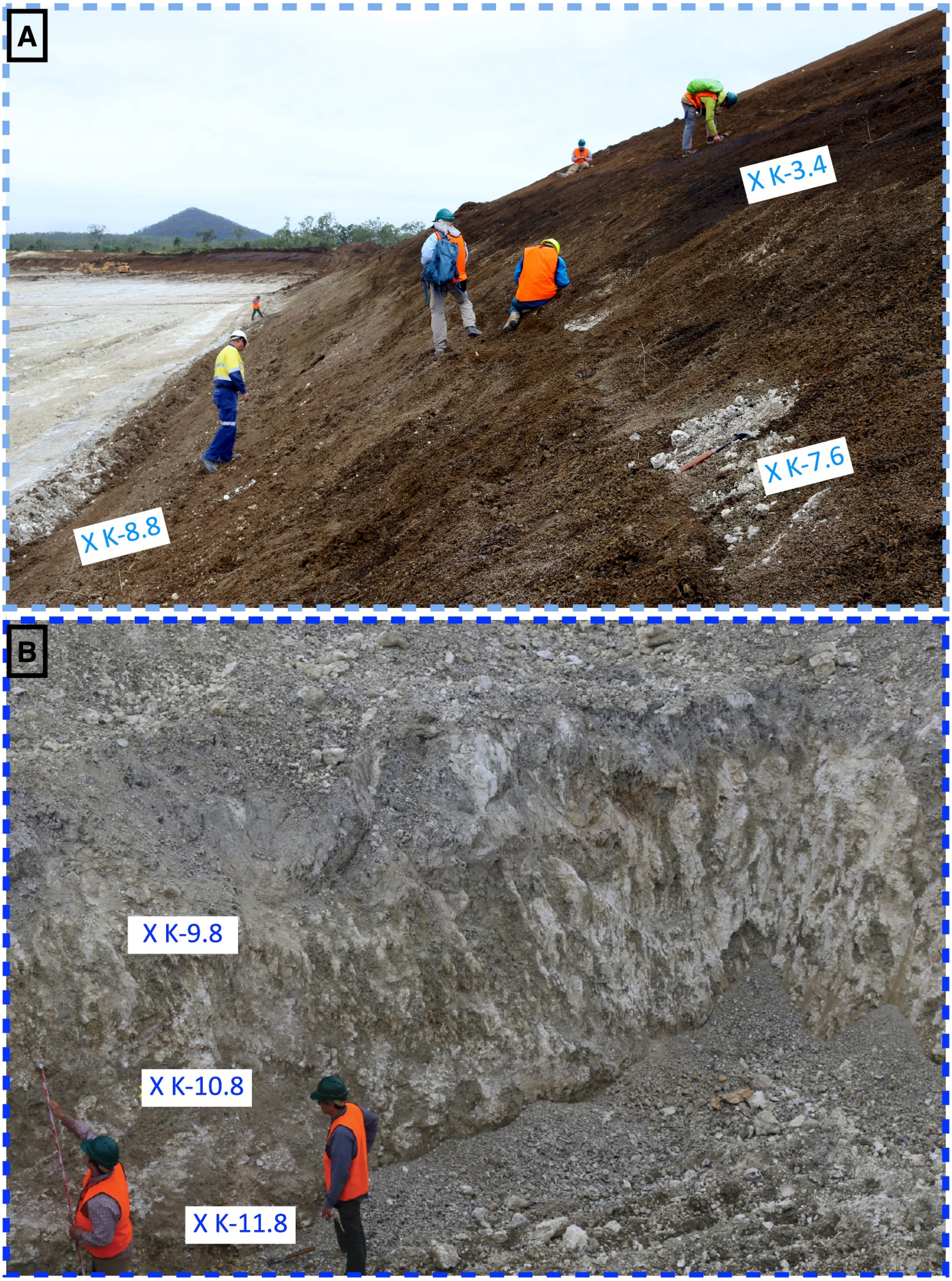

Figure 2. Field context of Kunwarara, Queensland, Australia. Field photos of Mg deposits in an exemplary vertisol (a - upper profile boxed in light blue, (b) lower profile boxed in dark blue) in Kunwarara where mining activities in the area have created terraces. The magnesites presented herein are formed when the arkosic sands undergo partial replacement by nodular magnesite, which forms from precipitation from Mg-rich groundwater. Fewer precipitation cycles at the top of the profile coupled with dissolution cycles due to rainwater infiltration produce weakly lithified magnesite nodules (a, b). Repeated precipitation cycles generate a magnesite cement at depth wherein magnesite spires develop through evaporation and pure Mg-carbonate nodules are also hosted (see sampling sites in b).

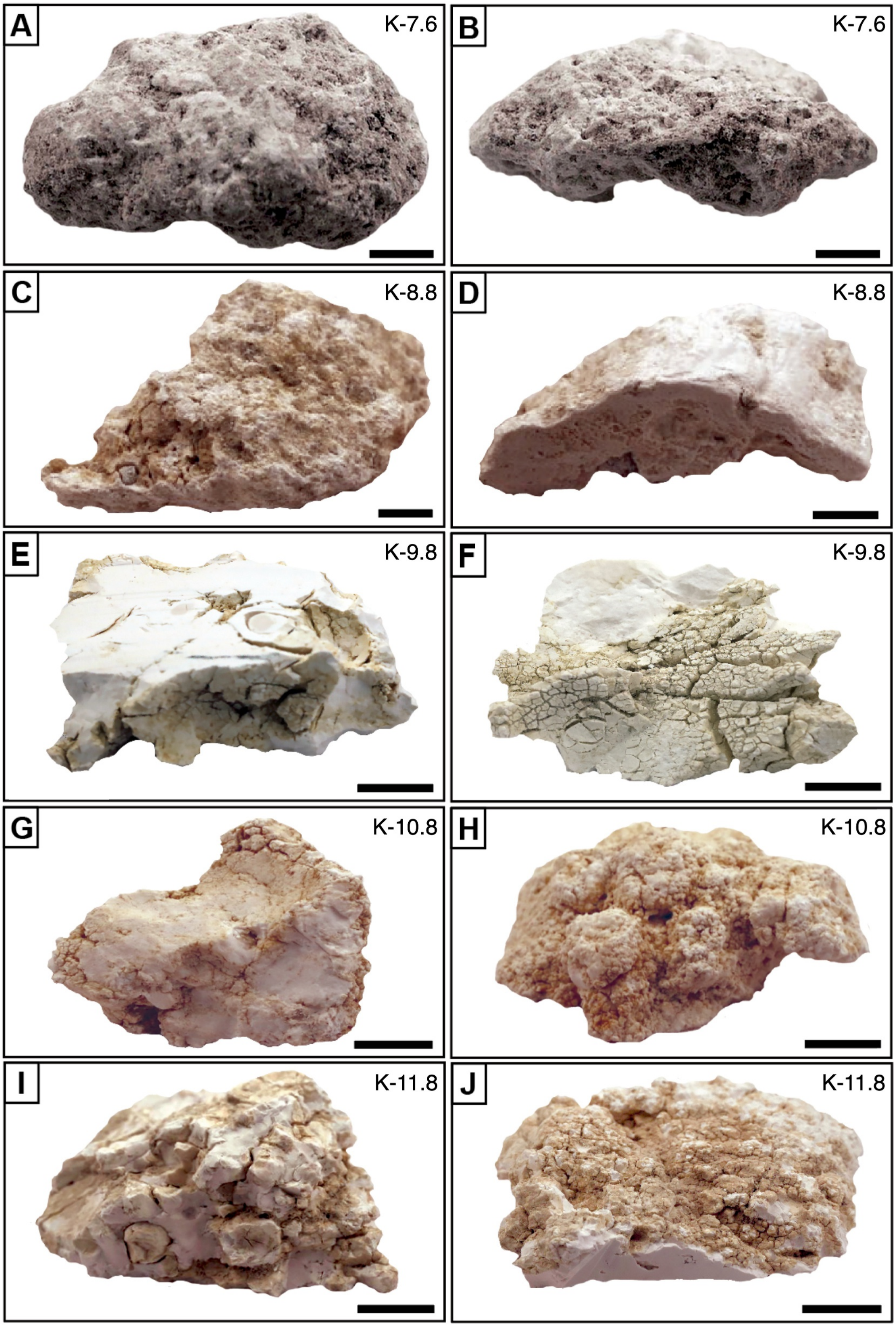

Figure 3. Carbonate nodule texture plates. Color-balanced images of magnesite hand samples with a 10 mm scale bar are arranged by position in the vertical profile beginning with K-7.6 (a, b) at the top followed by K-8.8 (c, d), K-9.8 (e, f), K-10.8 (g, h), and K-11.8 (i, j) at the bottom.

ray fluorescence (μXRF) with a Bruker M4 Tornado operating at 2 mbar vacuum with a 20 μm pixel size, 1 ms dwell time, and a rhodium X-ray tube powered to 50 kV and 600 μA.

3. Results

3.1. Composition and Occurrence of the Vertisol Hosted Sediments and Magnesites

3.1.1. Composition and Textural Relationships of Kunwarara Sediments

At the outcrop scale, the Kunwarara Vertisol examined is made up of an upper subsection (K-3.4, K-7.6, K-8.8) (Figure 2a, light blue box) and an offset lower subsection (K-9.8, K-10.8, K-11.8) (Figure 2b, dark blue box) separated by a mine pit terrace near the K-8.8 horizon. The top of the profile (∼0–6.8 m) is dark and contains cracks with manganese oxide nodules (K-3.4). With depth, the profile grades from dark brown (K-3.4) to a greenish-gray and brown clay horizon with millimeter-scale light colored carbonate nodules (K-7.6). In the lower subsection, the sediments are light gray sandy clays with manganese oxides precipitated along blocky cracks (K-8.8 and K-9.8), and weakly indurated clayey, silty, very fine sand (Figure 2, Table S1 and S2 in Supporting Information S1) hosting the most developed magnesite nodules (K-10.8 and K-11.8) (Figure 3).

In all samples, clay minerals were the dominant constituent of the sediments. XRD data indicated that the swelling clays were predominantly dioctahedral Al-smectites (i.e., montmorillonites) that were poorly ordered and contained little to no illite interlayers (Table S1 and S2, Figure S1 and S2 in Supporting Information S1). Small amounts of talc, illite, and kaolinite were also detected through the profile (Table S2 in Supporting Information S1). The upper subsection (Figure 2b) is also dominated by smectite, though quartz makes up a major mineralogic component (Table S2, Figure S1 and S2 in Supporting Information S1) as well. The reported quartz was likely authigenic as sand-sized grains in this horizon were rare (Figure 2). Minor dolomite and magnesite were detected by XRD in the sediment matrix of the upper samples, despite the low abundance of larger magnesite nodules (Figure 2, Figure S2, Table S2 in Supporting Information S1). Palygorskite was also detected in the sediment matrix (Figure S2, Table S2 in Supporting Information S1) at the bottom of the upper subsection (K-8.8) (Figure 2).

In the plane and polarized light images and SEM images, the dolomite was observed to form micron-scale discs (Figures 5a, 6a, 6c and 6f) and the magnesite formed micron-scale rhombohedra (Figures 5a, 6a and 6f). Other authigenic minerals, not detected in XRD data, were observed with SEM, including Mn-oxides coating clays and authigenic cerianite ((Ce, Th) O_2) (B and E, Figure S3 in Supporting Information S1). In the gradational horizon near the base of the upper subsection (K-7.6: 6.8–8.3 m bgs), wavy subhedral expandable clays overgrew an etched quartz grain. Also, potential fungal hyphae attached to ilmenite (Figure S3 in Supporting Information S1) were observed.

XRD, XRF, and SEM/EDS of the sediments showed that the sand in the lower subsection is quartz-dominated to arkosic in composition. In the sandy lower subsection (Figure 2b), the greatest proportion of quartz is present at the base and declines upwards. Quartz is present primarily as detrital silt and sand-sized grains, which are pitted and exhibit evidence of dissolution suggesting that their origin is partly detrital and alteration has occurred (Figure 5a). The lower sediment samples also contain variable amounts of additional immature detrital minerals (serpentine, plagioclase, potassium feldspar, and lizardite, Tables S1 and S2 in Supporting Information S1) that are not found in the upper portions of the profile. Clay minerals rim detrital grains, including quartz, feldspars, and heavy minerals (ilmenite and chromite which were observed with SEM but not abundant enough for XRD detection) (Figure S3 in Supporting Information S1). In addition to smectite, small amounts of palygorskite was detected in the lower subsection, and it declined in abundance from top to bottom (Tables S1 and S2, Figures S1 and S2 in Supporting Information S1). With SEM/EDS, both of these phases had microtextures of neoformed, authigenic clays including platey, wavy, or flakey smectite (Bohor & Hughes, 1971) and spikey, fibrous palygorskite (Kaplan et al., 2014) (Figure S3 in Supporting Information S1).

Swelling clays (smectite and mixed layer illite/smectite) dominate the composition of the upper profile subsection examined, followed by quartz (Figures S1 and S1, Table S2 in Supporting Information S1). The upper subsection sediment also contains variable proportions of lizardite, plagioclase, potassium feldspar, dolomite, magnesite, hematite and other clays (illite/mica, kaolinite, palygorskite, talc). Mn-oxides are also present as clay coatings. Dolomite, magnesite, and talc are only found in the sediment matrix of the upper subsection samples (Figure S3 in Supporting Information S1).

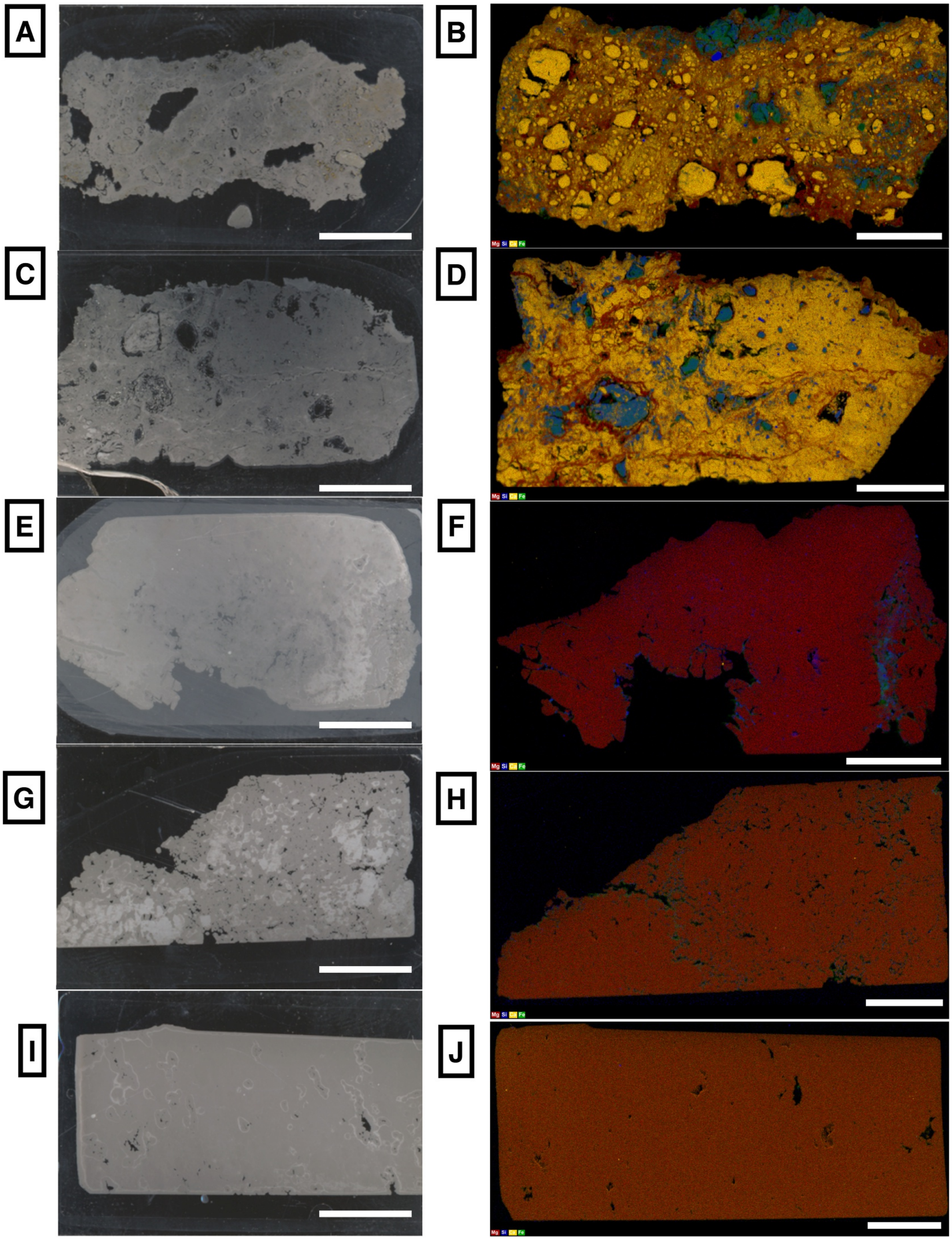

Figure 4. Carbonate thin section plates (27 mm × 42 mm) and x-ray fluorescence billet maps. Samples are arranged by position in the vertical profile beginning with K-7.6 (a, b) at the top followed by K-8.8 (c, d), K-9.8 (e, f), K-10.8 (g, h), and K-11.8 (i, j) at the bottom. Thin sections are in the left column and their corresponding x-ray fluorescence billet maps are in the right column with elemental legends in the lower left of each map. The following colors and labels are associated as follows: Red–magnesium (Mg), Blue–silica (Si), Yellow–calcium (Ca), Green–iron (Fe). The scale bar on all panels indicates 10 mm.

Overall, two major clay textures exist: (a) platey and wavy/flakey that we identify as smectite (Bohor & Hughes, 1971) and (b) spikey/fibrous, which we identify as palygorskite (Kaplan et al., 2014). At the bottom of the top subsection (K-8.8, Figure 2a), the presence of wavy subhedral expandable clays (kaolinite) over etched

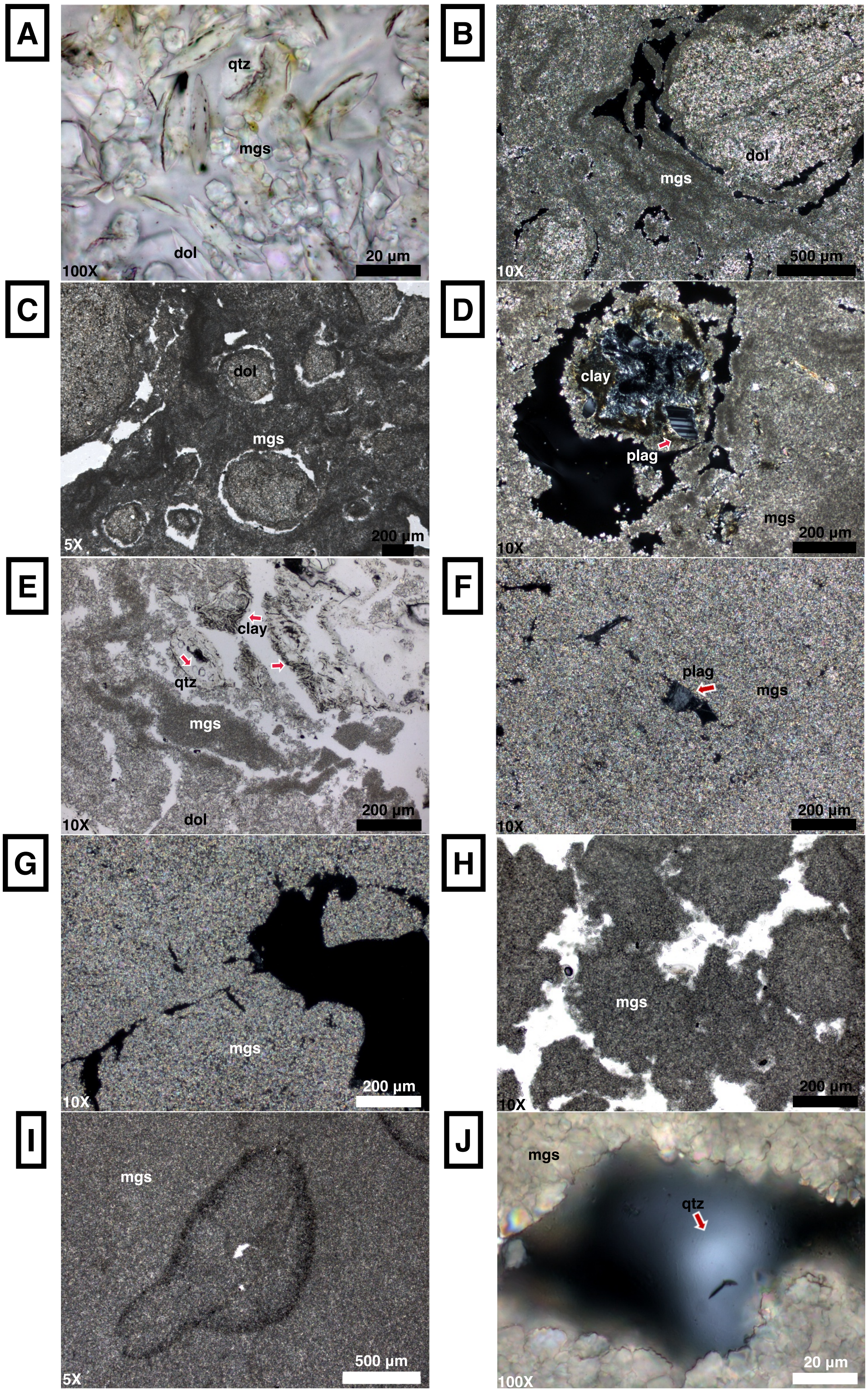
A
qtz
mgs
dol
100X
20 µm
B
dol
mgs
10X
500 µm
C
dol
mgs
5X
200 µm
D
clay
plag
mgs
10X
200 µm
E
clay
qtz
mgs
dol
10X
200 µm
F
plag
mgs
10X
200 µm
G
mgs
10X
200 µm
H
mgs
10X
200 µm
I
mgs
5X
500 µm
J
mgs
qtz
100X
20 µm

Figure 5.

quartz grains (Figure 5e) and Fe-Al clays bordered by other clays as well as Mg-carbonates (rhombohedral magnesite and dolomite, Figure S3 in Supporting Information S1). Magnesite from multiple depths also contains petrographic evidence for detrital quartz dissolution and associated K-feldspar (Figure 2). These observations suggest that the highest degree of weathering is near the top of the soil profile (Figure 7). Clay minerals rim detrital grains, including quartz and feldspar. In addition, rare earth elemental compositions of the sediments match magnesite found in the K-7.6 depth, suggesting an authigenic origin and neoformation for the overlying clays (Figure 7, Table S2 in Supporting Information S1).

3.2. Composition and Occurrence of the Kunwarara Magnesite Nodules

Magnesium carbonate occurs as a rare, micron-scale constituent of the uppermost black soil, but they form nodules that increase in size from millimeter-to decimeter-scale with depth below 6.8 m bgs (Figure 2). Magnesium carbonate exhibits variable morphologies, including cauliflower-like nodules, columnar concretions, and subhorizontal indurated horizons (Figure 3). Bulk powder XRD analyses determined that the samples were dolomitic magnesite at the base of the upper subsection (K-7.6 and K-8.8). Importantly, the Mg-carbonates occurrences were pure magnesite in the lower subsection (K-9.8, K-10.8, and K-11.8) (Figure 4, Figure S2 in Supporting Information S1).

In the uppermost magnesite-containing horizons (K-7.6 and K-8.8) of the upper subsection, Mg-carbonate is present as porous, friable, heterogeneous aggregates of magnesite and dolomite mixed with clay, oxide minerals, and siliciclastic sand grains (Figures 3 and 4, Figure S2 in Supporting Information S1). The aggregates are bright white and contain 100 μm to centimeter-scale glaebules that are light gray (Figures 3 and 4). Petrographic investigation reveals multiple types of glaebules (i.e., multidimensional entities in the soil matrix with a pedogenic origin) (Brewer & Sleeman, 1964) or micronodules hosted within the magnesite matrix. These multigenerational fabrics are composed of ∼2–4 μm subhedral rhombohedral magnesite crystals and discoidal or anhedral dolomite microcrystals (Figure 5); both phases exhibit nanoscale intercrystalline porosity. Magnesite micronodules have discrete edges that are defined by a rim of equant magnesite crystals that are generally smaller in size. By contrast, dolomite micronodules are composed of densely packed, limpid (clear) lensoid crystals. Dolomite lenses also occur within microcrystalline magnesite as well as scattered through the magnesite matrix. They are interspersed with microcrystalline magnesite, detrital phases, Fe-oxyhydroxides, and authigenic clays (Figures 5b–5d). Detrital quartz and plagioclase included in the aggregates have distinctive embayed margins and pitting associated with their dissolution, and other detrital components have been replaced by chalcedony or Fe-oxyhydroxides. Amorphous silica and chalcedony also line pores in magnesite aggregates. The uppermost magnesite (K-7.6) is porous, with void spaces and loosely packed phases visible with SEM/EDS (Figure 6a). At this depth, dolomite closely co-occurs with microcrystalline magnesite nodules that are a millimeter to 4 mm (Figures 4a, 4b and 5c), with both phases occasionally silicified (Figures 6a–6c). SEM/EDS analysis of the K-7.6 thin section reveals reaction fronts where microcrystalline magnesite (blue, Figures 6b and 6c) is overgrowing the discoidal dolomite that also contains embedded silicified grains. Microcrystalline magnesite is also observed to infill and to surround the discoidal dolomite, as well as to aggregate with itself and with dolomite discs (Figures 6b and 6c). Magnesite crystallites form sinuous, vermiform chains that anastomose throughout the aggregates (Figure 5b).

In the lower subsection (K-9.8, K-10.8, K-11.8), magnesite forms dense, bone-like, homogeneous, and mineralogically pure cauliflower-shaped nodules. The nodules are off-white to bright white in color and have a bulbous, hummocky surface with millimeter-scale pitting. The surfaces are further characterized by millimeter-to centimeter-scale reticular cracking (Figures 3e–3j). The nodules have a light brown exterior veneer of clay or amorphous silica (Figures 4e–4j). Magnesite is present as well-formed rhombohedral crystals, which are largely

Figure 5. Photomicrography of textures and relationships to other phases. Samples are arranged by position in the vertical profile beginning with K-7.6 (a, b, c) at the top followed by K-8.8 (d, e), K-9.8 (f, g), K-10.8 (h), and K-11.8 (i, j) at the bottom. Abbreviations found below are as follows: qtz–quartz, mgs–magnesite, dol–dolomite, plag–plagioclase. At the top of the profile, limpid dolomite crystals are found in association with smaller, rounder magnesite grains and quartz (a) as well as dolomite dominated nodules surrounded by magnesite veins (b, c). Complex relationships are present within the profile with variations in magnesite crystal morphology, size, and chemical composition are apparent across the different depth horizons. Millimeter-to nanometer-scale observations of mineral grains associated with carbonate and secondary silica are interpreted to indicate multiple formation steps, which include dissolution and pre-existing carbonate reprecipitation as magnesite is found overgrowing dolomite and being overgrown by dolomite. These phases are records of both carbonate and silicate mineral weathering processes that are traceable down to nanometer scales.

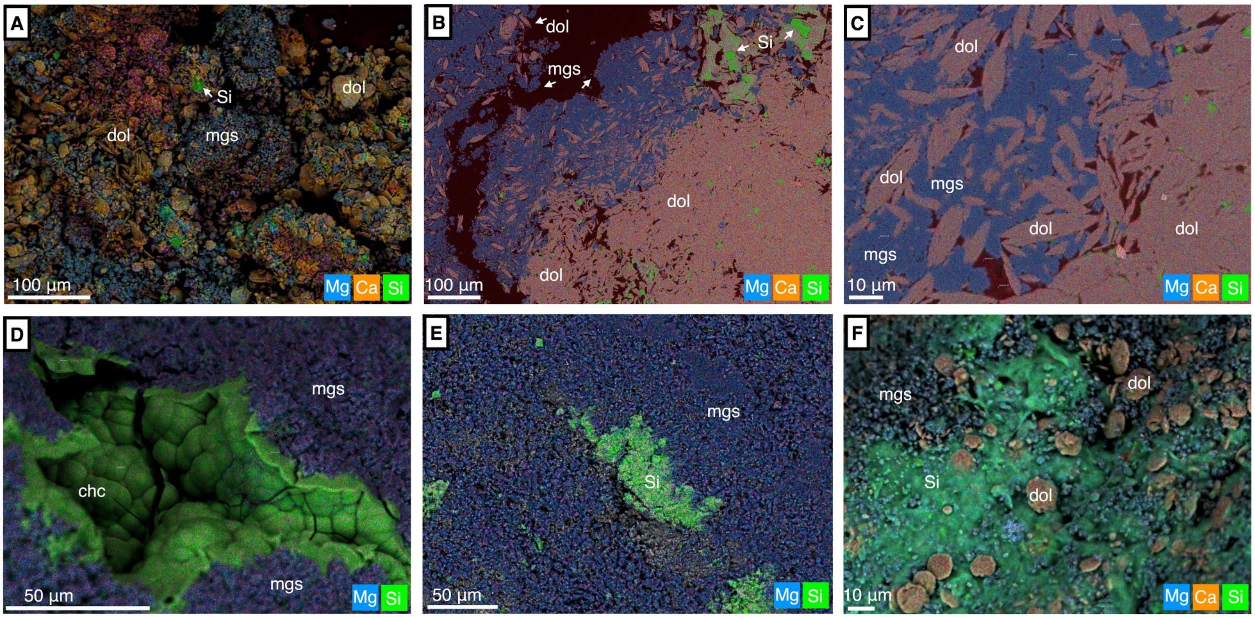

Figure 6. Scanning electron microscopy plate of magnesite—dolomite—silica textures and relationships. Magnesite (blue), dolomite (orange), and silica (green) phases in multiple samples are arranged by position in the vertical profile beginning with K-7.6 (a–rock chip, (b) thin section, (c) thin section) in the top row are contrasted to the base of the profile K-11.8 (d–rock chip, (e) rock chip) where silica infills voids of the cryptocrystalline magnesite cement as colloform chalcedony (d) and where silica-bearing phases become entrained in the magnesite cement (e). At intermediate depths (K-8.8), discoidal dolomite is embedded into the microcrystalline magnesite and both phases are silicified (F–rock chip).

devoid of inclusions (Figures 4e, g and 4i). The magnesite matrix consists of fine-grained, equant magnesite (approximately 5–20 μm in diameter) that occurs as both non-interlocking and interlocking crystals, which suggests moderate neomorphic recrystallization of primary magnesite (Figures 5f–5j). Despite the macroscopically homogeneous appearance of magnesite found in the lower subsection (Figure 2b), there are small micronodules (approximately 10–20 μm) that are subtle yet made up of similarly fine-grained equant magnesite crystals displaying grain coarsening at the margins of the micronodules (Figure 5c). These relationships differ from those in the upper subsection wherein finer coatings of magnesite exist at the micronodule margins (Figures 4a–4d and 5c) and as the anastomosing phase.

The topmost sample from the lower subsection (K-9.8) contained rare detrital quartz, plagioclase, and feldspar as well as minor pore-lining chalcedony (Figure 5f). This sample also indicated that magnesite was replacing plagioclase, following the plagioclase twinning through replacement and leaving moldic pores (Figures 6d and 6e), that is, porosity created by a pre-existing constituent dissolving. In the deeper nodules (K-10.8, K-11.8), microcrystalline magnesite was observed as equant, tightly packed grains with 100 micron-to millimeter-scale irregular pores that have dark halos (Figures 4i, 4j and 5i). These colored halos may be discolored where plucked and/or soluble grains left pores through which fluids may have infiltrated, after the formation of the microcrystalline magnesite.

4. Formation and Pedogenic Alteration of Mg-Carbonate Nodules and a Groundwater Magnecrete

Observations across multiple spatial scales reveal that the quartz and arkosic sands found at the base of the profile are the result of Neogene/Quaternary fluvial deposition. These sediments were subject to diagenesis and chemical weathering to produce the authigenic clay and the Mg-carbonate at Kunwarara. Millimeter-to nanometer-scale observations of mineral grains associated with carbonate and secondary silica indicate multiple formation steps, which include dissolution and pre-existing carbonate reprecipitation as magnesite is found overgrowing dolomite and being overgrown by dolomite. These phases are records of both carbonate and silicate mineral weathering processes down to nanometer scales, as carbonate weathering produces pores during Mg dissolution. By contrast, silicates weather incongruently, producing alteration minerals and releasing dissolved Si species.

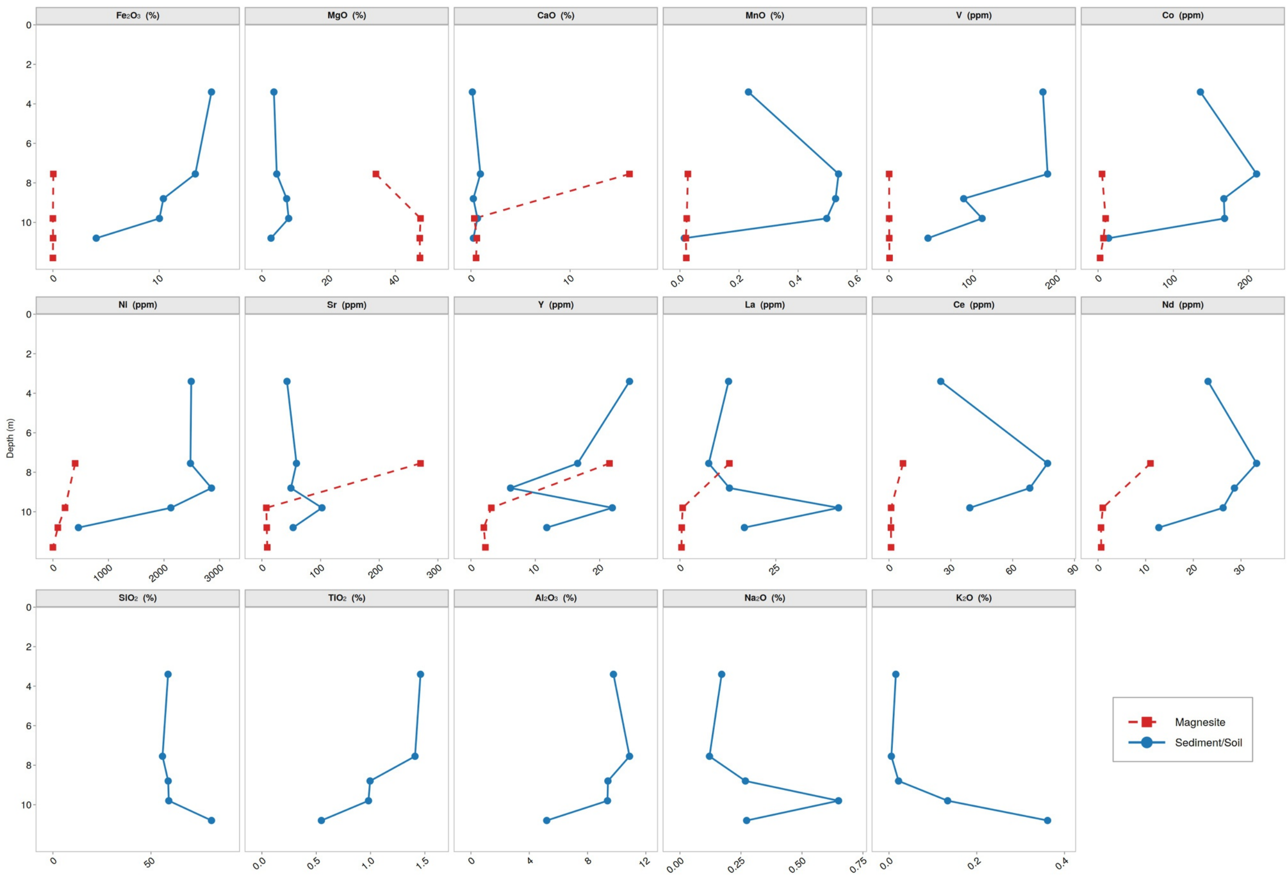

Figure 7. Rare earth element abundances in magnesites (K-7.6, K-8.8, K-9.8, K-10.8, K-11.8) and the associated sediments (K-3.4, K-7.6, K-8.8, K-9.8, K-10.8) over a depth profile (figure modified from Swindle, Vasconcelos, Dimarco, et al., 2025, Swindle, Vasconcelos, Dalleska, et al., 2025). Depth trends suggest that there is an increasing influence of the elements coming from the dissolving sands as the depth and amount of magnesite decrease. Magnesite is growing progressively from solutions coming from the bottom of the profile, and as Mg derived from the ultramafic source rocks increases, the REE signature from the dissolving sediments decreases.

The Vertisol identified at Kunwarara is characterized by a series of soil horizons wherein multiple types of magnesite have co-developed with the surrounding sediments. There is an intimate relationship between the magnesite and clay, suggesting that both magnesite and clay are neoformed within the profile from weathering of arkosic sands via carbonation by Mg-rich fluids. The Kunwarara profile is a site of Mg accumulation where few primary Mg-bearing phases occur and magnesite increases in purity while authigenic silica phases decrease in abundance with depth (Figure 4, Figure S2 in Supporting Information S1). Pedogenic carbonate occurs overlying groundwater-formed magnesite that developed via downward alteration. Mg-carbonate is present as porous friable magnesite (upper subsection of Figures 2a and 3) and denser magnesite (lower subsection of Figures 2b and 3). Pore architecture controls the connectivity (i.e., permeability of the pore network), and a range of pore structures were observed. We report enhanced pore structures and permeability at the top of the profile (K-7.6) and reduced pore sizes and predominantly nano-to microscale intercrystalline porosity deeper belowground (K-8.8 to K-11.8, Figures 3 and 4).

Our petrographic and spectroscopic results suggest that magnesite precipitates as Mg^{2+}- and CO_3^{2-}–rich groundwaters move upward through the soil profile, with magnesite recrystallizing and becoming more pure at the base of the profile with each precipitation event. At the top of the profile, magnesite overgrows dolomite and fills voids left by dissolving clay. Dolomite may be formed late in the upward paragenesis, as initially $Mg^{+2}_{(aq)}$-rich groundwaters became progressively enriched in $Ca^{+2}_{(aq)}$. Aqueous $Ca^{+2}_{(aq)}$ could have reacted with early formed magnesite or Mg-rich groundwater, producing late-stage dolomite. In addition, aqueous $Na^{+1}_{(aq)}$ and $K^{+1}_{(aq)}$ could have combined with dissolved H_4SiO_4 produced by the etching and dissolution of detrital quartz to produce the authigenic clay minerals observed. Authigenic aluminous clays may also have formed in situ by the

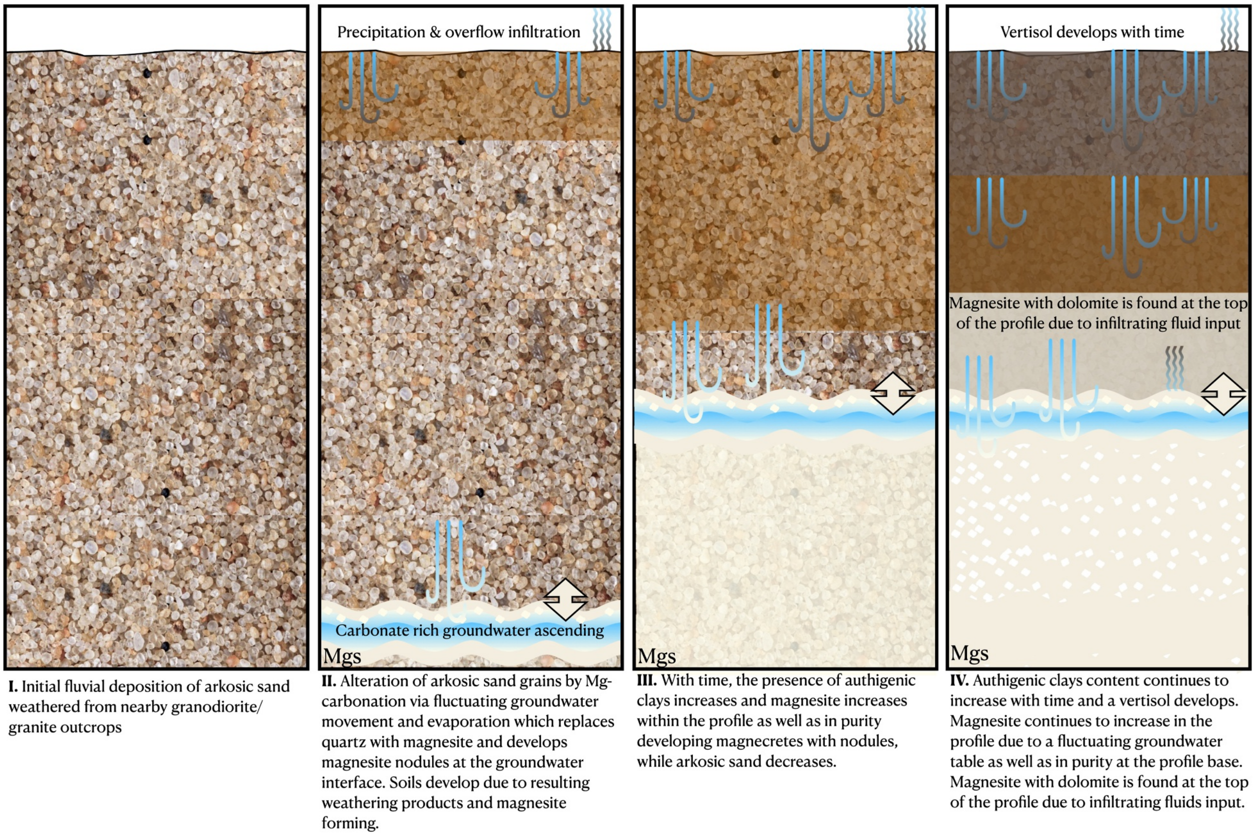

Figure 8. Conceptual diagram for the formation of magnesite and the sediments found in the sampled vertisol. Stages I-IV indicate formation and development through time. Wavy blue lines indicate meteoric water infiltration. Illustration of blue lines (sets of 3) colored with blue to brown indicates infiltration throughout the vertical profile. Illustration of blue lines (sets of 3) colored with blue to white and shown with a white arrow indicates groundwater ascending and fluctuating groundwater movement.

incongruent dissolution of feldspars. The discoidal dolomite texture could be a result of precipitating dolomite from an aqueous hydromagnesite solution that was enriched in Ca from surficial sources.

Fluctuating fluid conditions are inferred from the aforementioned petrographic observations indicating that the magnesite becomes altered through dissolution and recrystallization processes (Figure 5), which are hypothesized to be ultimately driven by fluctuations in the water table that impart variations in soil pH (Rezanezhad et al., 2014; Zhang & Furman, 2021), changing oxygen conditions (Peralta et al., 2014; Pett-Ridge & Firestone, 2005; Rubol et al., 2012), and the availability of reactive mineral or organic phases (Fischel et al., 2023; Power et al., 2017). The presence and development of variably sized Mg-carbonate glaebules within Mg-carbonate nodules would also support fluctuating fluid conditions (Brewer & Sleeman, 1964). These hydrologic changes result in variations in magnesite crystal morphology, size, and chemical composition across different soil horizons as well as in the accessory phases, which are observed (Figures 3, 5, 6 and 7) and have been evaluated with laboratory studies (Deelman & Eindhoven, 1999; Dos Anjos et al., 2011).

4.1. Evolution of a Mg-Carbonate-Bearing and Vertisol Capped Sedimentary Succession

The dark smectite soil horizon may have multiple roles in the evolution of the precipitating phases within the underlying Kunwawara sedimentary succession. Multiple hypotheses are presented that are based on how calcrete profiles develop (Alonso-Zarza et al., 1998; Alonso-Zarza & Silva, 2002) and how spatial transitions of alluvial, palustrine, and lacustrine deposits in alluvial/floodplain environments (Alonso-Zarza, 2003) influence the resulting profiles, as well as based on foundational theory of waters within watersheds (Freeze, 1974; Smith et al., 2017; Stegen et al., 2025). A top-down hypothesis is that the overlying clay layer (made up of predominantly shrink-swell clays) has developed above the magnesite and sand horizons during weathering of arkosic sand by down-traveling meteoric waters, which dissolves the underlying magnesites and arkosic sand grains and produces authigenic clays. When the clays swell, they may act as a capping layer to the lower lithologies. This cap could limit the disintegration of the friable magnesite at the top of the profile and enable enhanced "hotspot" biogeochemical activity via microbial activity within the vadose zone (Kuzyakov & Blagodatskaya, 2015; McClain et al., 2003), allowing pCO_2 to build up and then become a destructive agent to magnesite (Leon et al., 2014; Ning et al., 2025). Alternatively, the cap could preserve the initial conditions and alteration extent because the clay unit caps the dolomite and magnesite units, thus limiting precipitation and fluid flow. A second hypothesis for the role of the overlying smectite layer is that it supplies particulate or dissolved organic matter to the subsurface, allowing pedogenic solutions to infiltrate downwards when the clays shrink and supporting the development of magnesite at depth because organic surfaces have been shown to facilitate and potentially control the formation of magnesite at low temperatures (Power et al., 2017, 2019).

A third hypothesis is that the smectitic soil formed as ascending groundwater dissolved the arkosic sand matrix at depth and carried Si phases to shallower depths, where evaporation of the ascending groundwater precipitated magnesite together with authigenic clay minerals. Salinity changes have major impacts on the swell ability of shrink-swell clays, their exchange capacity (Carroll & Starkey, 1958) and the molecular kinetics of clay surfaces (Cama & Ganor, 2015). Figure 7 and Table S2 in Supporting Information S1 illustrate the geochemical relationship between the magnesite and clays (Figure 2). Rare earth element data reported by Swindle, Vasconcelos, Dimarco, et al. (2025), Swindle, Vasconcelos, Dalleska, et al. (2025) indicate that only the shallowest magnesite shows elemental signatures of the host sediments, while deeper magnesite samples show element trends that are consistent with ultramafic rock-derived fluids (Figure 7). These findings indicate that the Mg-rich, ultramafic-derived groundwater repeatedly recrystallized the deepest, most mature magnesite. The least mature, initial magnesite and dolomite at the top of the profile derives largely from the residue of the dissolving sediments. Figure 8 shows a conceptual sequence of this evolution of terrestrial through time as Stages I-IV, which is consistent with prior calcrete evolutionary model sequences (Alonso-Zarza & Silva, 2002; Alonso-Zarza, 2003; Alonso-Zarza et al., 1998; Gile et al., 1966). These findings also support the third hypothesis for the origin of the swelling clays in the overlying vertisol: upward-migrating groundwater dissolves arkosic sand and precipitates magnesite, followed by dolomite and silica phases enabled by accumulation of solutes as the sand dissolves.

Vertical mobility and crack development in the vertisol over differing timescales could be induced by an interplay of wet-dry conditions driven by seasonal fluctuations as well as more intense climatic regime changes (Khitrov, 2016; Miller et al., 2010). Vertisols that contain abundant shrink-swell clay develop in tropical and subtropical climates with pronounced wet and dry seasons (Ahmad, 1983; Kovda, 2020). These wet and dry seasons drive seasonal changes in the local groundwater composition that influences the formation of the Kunwarara vertisols hosting accumulated magnesite. The multiple authigenic mineral phases and evidence for repeated episodes of mineral dissolution-reprecipitation within the Kunwarara magnesite nodules are both consistent with formation from episodic and recurring groundwater upwelling. Figure 8 summarizes the stages of accumulation and diagenesis of magnesite within the Kunwarara Vertisol observed. This multi-stage figure illustrates how the Vertisol and carbonates evolve with the composition of the local groundwaters that are dominated by bicarbonate and magnesium and change through variations in evaporation, evapotranspiration, and Ca-rich surface water influx. While this work determines that these petrographic fabrics are altered by aqueous fluids which is confirmed by past isotopic and geochemical work (Oskierski et al., 2013; Swindle, Vasconcelos, Dalleska, et al., 2025), a literature review of the composition of surficial waters and groundwaters of the area in the past 50 years (McNeil & Raymond, 2013) also suggests that seasonal fluctuations controls the water composition delivered to the Vertisol. However, it is acknowledged that rainfall in Queensland is the product of interannual and decadal variability (Klingaman, 2012) though tracing the water source for this study is limited as this work is focused on the formation and alteration of magnesite nodules from Kunwarara, Queensland, Australia found throughout in a Vertisol profile at a point in time.

Microscopy reveals petrographic evidence of pedogenic overprinting affecting the Mg-clay minerals (Figure S2 in Supporting Information S1) as well as the carbonates (Figures 3 and 4). Within the Mg-clays, replacement by silica (quartz, chalcedony) and carbonates (dolomite and magnesite) is common. We also observe a homogenization of the magnesite textures into a laminar texture (K-10.8) (Figure 3), which may have occurred during the diagenetic compaction process (Kadir et al., 2018) or as a result of prior microbial activity in situ (Eren et al., 2018). At Kunwarara, the multiple clay phases are interpreted to be authigenically formed. Laboratory experiments have demonstrated low-temperature magnesite precipitation occurring with fluctuating pH conditions (Hobbs & Xu, 2020) or with densely packed active carbon sites (i.e., available carboxyl groups), which bind yet also dehydrate Mg^{2+} ions from solutions (Power et al., 2017). Carbon speciation can influence the process of magnesite precipitation as well as the magnesite habit, both of which may be occurring within this profile. Montes-Hernandez et al. (2020) indicated that the presence of functionalized organic groups can reduce the energetic barriers during magnesite nucleation.

4.2. Comparison of Kunwarara Magnesite Nodules to Other Mg-Carbonate Nodules Documented on Earth

The complex petrographic fabrics observed within the Kunwarara magnesite nodules suggest that the magnesite itself has undergone repeated episodes of wetting/drying and dissolution/precipitation. Evidence for magnesite dehydration is most easily observed on the surfaces of nodules, which commonly show a 0.5 cm-scale polygonal pattern of cracks (Figure 3). These cracks can narrow with depth or retain the same width several millimeters into the nodule. Such polygonal cracking is indicative of contraction with water loss, suggesting potential dehydration of an originally hydrated $MgCO_3$ phase or the nodules growing/coalescing, or even dissolving. The circum-granular fractures throughout the nodular fabric are also consistent with soil motion during growth (i.e., compaction, clay shrink/swell, root bioturbation, etc.) (Alonso-Zarza & Wright, 2010; Wright, 2007) and plasmic zone textures (Wright, 1982). Apparent termination of equal-width cracks at an equivalent depth in the nodule may also indicate dehydration of just the most recent material added to the nodule during growth.

Mg-carbonate nodules have been documented in multiple localities on Earth, and some localities have comparable textures or similarities to Kunwarara. These localities include weathering-derived cryptocrystalline magnesite nodules and veins in the Attunga magnesite deposit of the Great Serpentinite Belt, Australia associated with nearby ultramafics (Oskierski et al., 2013), and similar to the Kunwarara magnesite nodules in its proximity to ultramafics and weathering-derived regime. The Upper Permian Gröden Formation of the Northern Calcareous Alps, Austria is another Mg-carbonate nodule hosting locality with magnesite nodules in alluvial fan and playa lake sediments, deposited in intermontane basins (Spötl & Burns, 1994). These hollow magnesite nodules (up to 10 cm diameter, often filled with aragonite) are found in massive red siltstones and shales. Magnesite cements reported from the Sandtal Mühlbachgraben and Kundler Klamm sections were micritic (<4 μm) and microsparitic (5–20 μm). Like the Kunwarara magnesites, multiple generations of magnesite were also observed with SEM/EDS and under SEM, the micrites consisted of tightly packed magnesite crystals (2-4 μm in size)—similar to the bottom lower subsection magnesites (K-10.8, K-11.8, Figures 2b and 4). However unlike Kunwarara, pedogenic structures like laminar fabrics were not reported in the Upper Permian Groden Formation magnesites (Figure 4).

4.3. Comparison of the Kunwarara Magnecrete to Other Calcretes Documented on Earth

The magnesite accumulation at Kunwarara shares many features with groundwater calcretes in other terrestrial settings. The location of the magnecrete horizon reflects the balance between downward carbonate redistribution by the leaching of dissolved carbonate in a percolating acidic soil solution, and accumulation resulting from capillary action from Mg-rich alkaline groundwater near the top of the water table moving upwards. The location of this zone is controlled by the extent of the wetting front following rainfall events (Goudie, 1983). Lateral transfers of carbonate-rich groundwater result in carbonate mineral accumulation displaced from the site of weathering (Arakel, 1986; Bachman & Machette, 1977; Goudie, 1983), so carbonate precipitation occurs by replacing sediments near the groundwater table (Alonso-Zarza, 2003; McLaren & Gardner, 2004; Nash & McLaren, 2003).

Regional water survey data based on 13,000 water quality samples aggregated over 50 years (McNeil & Raymond, 2013) identifying that waters in the area drain basaltic/ultramafic provenances and are Mg+ and HCO3-dominated, geochemical data for both the matrix and the magnesite (Figure 8) (Swindle, Vasconcelos, Dalleska, et al., 2025), and morphological interpretations from this work suggest that this profile is a moderately alkaline weak-leaching environment wherein Si may be sourced from the detrital arkosic sands that predate the formation of magnesite. Detrital plagioclase or exogenous sources encountered during the transport of rainwater within the catchment, infiltrating into the sediment profile may source the Ca found within the top of the profile, which has undergone multiple aqueous alteration events. Under alkaline aqueous conditions, Mg (as aqueous Mg^{+2}) and Si (as H_4SiO_4) are soluble and high CO_3^{-2} concentrations are possible. Other Australian localities have also reported an increase in Mg content of Ca-Mg carbonates with depth (McQueen et al., 1999; Milnes & Hutton, 1983).

5. Linkages to Mg-Carbonate and Fe/Mg Clay Detections on Mars

Carbonates have been well-documented in Martian weathering profiles (Bultel et al., 2019) and their chemical composition has predominantly been reported as Fe/Mg- or Mg-carbonates from orbital (Ehlmann et al., 2008; Tarnas et al., 2021) and in situ observations (Clavé et al., 2023; Corpolongo et al., 2023; Jones et al., 2026; Scheller et al., 2022; Shumway et al., 2025; Tutolo et al., 2025; Williford et al., 2026). Pedogenesis had been suggested as a formation mechanism to produce vertical mineralogical variation observed on the order of meter to decameter scales (Gaudin et al., 2011) in the ExoMars Oxia Planum landing site (Brossier et al., 2022; Mandon et al., 2020) and hectameter scales in the previously proposed Mawrth Vallis landing site (Bishop et al., 2008; Loizeau et al., 2015) for Mars 2020.

This study documents and elucidates the processes that have led to the formation and preservation of a unique sediment-hosted magnecrete. This work provides a valuable example of terrestrial carbonate formation in a weathering sequence that may be useful as additional Mg-carbonate phases are revealed through ongoing orbital and rover-based investigations to better understand how these mineral phases found may have formed on Mars. This work is well-timed with the detection of multiple Mg-carbonate phases in multiple geologic units found on the Mars 2020 mission and for upcoming rover-based exploration in Oxia Planum by the ExoMars mission. These findings have implications for understanding the Mg-carbonate bearing units of Jezero crater and in other localities on Mars. More generally, Mg-carbonates may also preserve evidence of Mars' past water cycle, offering valuable hydrologic insights that could be returned to Earth through a potential Mars Sample Return Mission.

Martian Mg-carbonates have the potential to record past water-rock interactions, signs of ancient life, and environment conditions. This study establishes that magnesite forms in pedogenic weathering profiles on Earth, thereby supporting the formation of Mg-carbonate dominated cements at depth (i.e., magnecretes). Few deposits of magnesium-dominated calcretes (i.e., magnecretes) have been well-documented and characterized in the world. Recent reviews of the planetary formation of Mg-carbonates relevant for Mars do not mention pedogenic formation (Scheller et al., 2021). In addition, pedogenic carbonate reviews (Khalidy et al., 2022; Ning et al., 2025) exclude magnesite forming through this mechanism, so this work fulfills an important gap in both earth and planetary science literature. Though these magnecretes may be similar in some textures and fabrics observed in other calcretes worldwide, the limpid crystals with a higher calcium magnesite composition are unique and to our knowledge have not been reported before.

5.1. Orbital and In Situ Observations

Orbital and rover-based observations have revealed Mg-carbonate detections in the Nili Fossae region (Ehlmann et al., 2008) as well as in the Jezero crater watershed, the Margin Unit of Jezero crater (Horgan et al., 2020; Phua et al., 2024; Tarnas et al., 2021), and the Delta Front Unit at Hogwallow Flats (Kalucha et al., 2024). Mg-carbonates and Fe/Mg clays have also been detected with orbital and in situ observations made in Gusev crater within Columbia Hills at the Comanche outcrop by the Mars Exploration Rover Spirit (Morris et al., 2010). They have also been identified in Gale crater at the Mg-sulfate unit (Tutolo et al., 2025), lower strata (Leshin et al., 2013), and in aeolian deposits (Stern et al., 2018) by the Mars Science Laboratory Curiosity rover. Other localities where they are observed include Oxia Planum bedrock outcrops (Lucia Mandon et al., 2021), in Arabia Terra within McLaughlin Crater (Michalski et al., 2013), and in Vastitas Borealis within martian regolith by the Mars Phoenix lander (Sutter et al., 2012). Additional localities may be present globally, since the presence of sulfate has been shown to obscure orbital carbonate detections on the martian surface (Sheppard et al., 2025). Mg-carbonate detections have also been documented within the Martian meteorite Allan Hills 84,001 (Scott et al., 1998). Their textures have included zoned concretion rims, veins, void fillings, and multi-generational assemblages (Corrigan & Harvey, 2004; Halevy et al., 2011; Treiman, 1995), which indicate complex histories of formation and alteration.

5.2. Kunwarara as a Planetary Analog for Mg-Carbonate Detections on Mars?

This site is a useful planetary analog for the aforementioned Martian Mg-carbonate detections for the following reasons. (a) This site hosts an extensive vertical weathering profile, which has been well-documented on Mars. (b) This site also hosts carbonates with an Mg-carbonate geochemical composition, which has been the predominant form of carbonate detected from orbital and in situ observations on Mars. (c) Kunwarara hosts grain sizes that are the same size as those reported in Jezero crater (~1 mm) (Farley & Stack, 2024; Williford et al., 2026). (d) The

Journal of Geophysical Research: Planets 10.1029/2026JE009660

Vertisol investigated has undergone alteration by Mg-dominated fluids (i.e., fluids that have interacted with ultramafic/mafic lithologies). (e) This locality hosts magnesite-bearing cements, like observations from Jezero crater (Farley & Stack, 2024; Williford et al., 2026). (f) Kunwarara has undergone extensive episodic wet-dry cycling like the Martian surface more generally and Jezero crater, in particular. (g) This study indicates that both surficial and subsurface waters have influenced the formation and alteration of the magnesite described. Ehlmann et al., 2008; Scheller et al., 2021 have suggested these components to form the Mg-carbonates on Mars. (h) The accumulations of Mg-carbonate minerals associated with authigenic phyllosilicates identified indicate that Mg-carbonate could have formed from low-temperature processes such as pedogenesis (Sutter et al., 2012) or groundwater alteration (Kite et al., 2025; Michalski et al., 2013), as previously hypothesized.

5.3. Kunwarara as a Planetary Analog–Differing From Jezero Crater, Mars?

While felsic material has been found on the Crater Rim of Jezero crater, Mars (Liu et al., 2026), the primary mineralogy of sand grains at Kunwarara (felsic) differs from predominant grain mineralogy detected on Mars (basaltic to ultramafic). Geochemical grain compositional differences may influence chemical interactions on the grain surfaces as well as the neoformed phases found and the sources of $Mg+$ in the system. The Vertisol at Kunwarara had felsic grains present, which were deposited by fluvial processes.

This site may be a debatable analog to localities on Mars because a major Mg-carbonate unit known as the Margin Unit in Jezero crater has a debatable origin (Cardarelli et al., 2026; Clavé et al., 2026; Jones et al., 2026; Williford et al., 2026), with a fluvial origin considered for the entire unit or just for the Eastern Margin Unit. A second reason this site may be a debatable analog: this site has similar grain sizes to those reported in the Margin Unit (Williford et al., 2025) and likely in alteration history (i.e., altered by waters draining a mixed basaltic/ultramafic and/or ultramafic provenance producing alkaline fluids), though the formation and emplacement mechanisms may differ for the Margin Unit grains and the Kunwarara grains per Williford et al., 2025.

Overall, the Kunwarara, Queensland, Australia site expands the literature on the formation and evolution of large-scale Mg-carbonate deposits that are relevant to Mg-carbonate detections made on Mars—in fluvial settings as well as in weathering profiles which have experienced fluctuating hydrologic conditions. In situ observations combined with the collection of two drill-cores within the Mg-carbonate dominated Margin unit for sample-return reveal the importance of studying large-scale Mg-carbonate deposits (i.e., Kunwarara, QLD, Australia) as a useful Mars analog. Results from this study serve as a reference that can provide context to paleoenvironmental information preserved in Mg-carbonates and clays forming near the martian surface.

5.4. Implications

Inferences from the mineralogy and textural relationships preserved in the Kunwarara sediment profile (Figure 8) may have significant implications for understanding the chemical composition, formation, water-rock interactions, and geologic history of Mg-carbonate bearing localities. While analog sites cannot exactly replicate the complex and unique conditions found on Mars, this study provides useful insights on the extent to which Mg-carbonates and corresponding clay minerals capture stages of fluid-rock interactions and alteration processes. Future investigations might focus on expanding the sampling range and simulations conducted at Kunwarara to encompass a broader array of Martian conditions and rover-like analyses for improved comparative study. This study supports the proposition that magnecretes as well as calcretes (Alonso-Zarza & Silva, 2002) develop as a result of an interplay of pedogenesis, groundwater precipitation, and episodic alteration that are visible in the depth horizons as well as down to the centimeter to micrometer scales. This work expands the environments and formation mechanisms that could be responsible for widespread Mg-carbonate orbital detections and the search for possible biosignatures that might be preserved in Mg-carbonates on Mars.

6. Conclusions

The Kunwarara Vertisol records various stages of magnesite formation and alteration. Identified microtextures and mineralogy within both the magnesite and the matrix track the timing, intensity, and relative relationships of the presented processes—predominantly magnesite authigenesis and diagenesis (i.e., precipitation-dissolution) through dynamic eluvial-illuvial activity occurring in the matrix. Textural evidence indicates that rising, ultramafic-derived groundwaters precipitate in the capillary zone of alluvial sediments that have developed a vertisol profile after undergoing multiple stages of precipitation-dissolution. The elemental constituents are sourced from weathering of the Princhester Serpentinite and subsurface lateral flow of groundwater enriched in magnesium and bicarbonate. Our analyses revealed evidence of upward movement of groundwater into the Vertisol profile and movement within the vertical profile.

Moreover, within this system, the oldest, most evolved diagenetic magnesite horizon has developed and been preserved at the base of the profile as a Mg-carbonate cement. It forms dense nodules with little to no macroscopic pore-space and has an intimate formational relationship with Si that may also aid in its preservation. Petrographic results indicate that the dissolution of arkosic sands was coupled with precipitation of secondary silica and clays. A pedogenic dolomite-rich horizon above the magnesites developed as the fluid previously rich in magnesium and bicarbonate evolved toward a more Ca-rich composition because magnesite and Mg-clay phases remove magnesium, while the dissolution of detrital plagioclase releases calcium. These precipitated Mg-carbonate phases, containing Mg-rich dolomite and magnesite, undergo greater destruction and alteration due to infiltrating surficial waters.

Conflict of Interest

The authors declare no conflicts of interest relevant to this study.

Availability Statement

Original authors are referenced for imagery or data that are presented here, when approporiate. For the study data presented, the data can be found in the supplement as data tables and figures as well as within a Zenodo repository (https://doi.org/10.5281/zenodo.21267544).

Acknowledgments
Support for E.L. Cardarelli was provided by NASA Grant 80NM0018D0004 through the Jet Propulsion Laboratory, California Institute of Technology. This work was supported by the Simons Foundation Grant 668346 awarded to J. Grotzinger and the National Science Foundation Graduate Research Fellowship Grant (DGE-1745301) awarded to C. Swindle.

References

Ahmad, N. (1983). Chapter 3 vertisols. In *Developments in soil science* (Vol. 11, pp. 91–123). Elsevier. https://doi.org/10.1016/S0166-2481(08)70614-7

Alonso-Zarza, A. M. (2003). Palaeoenvironmental significance of palustrine carbonates and calcretes in the geological record. *Earth-Science Reviews*, *60*(3–4), 261–298. https://doi.org/10.1016/S0012-8252(02)00106-X

Alonso-Zarza, A. M., & Silva, P. G. (2002). Quaternary laminar calcretes with bee nests: Evidences of small-scale climatic fluctuations, eastern Canary Islands, Spain. *Palaeogeography, Palaeoclimatology, Palaeoecology*, *178*(1–2), 119–135. https://doi.org/10.1016/S0031-0182(01)00405-9

Alonso-Zarza, A. M., Silva, P. G., Goy, J. L., & Zazo, C. (1998). Fan-surface dynamics and biogenic calcrete development: Interactions during ultimate phases of fan evolution in the semiarid SE Spain (Murcia). *Geomorphology*, *24*(2–3), 147–167. https://doi.org/10.1016/S0169-555X(98)00022-1

Alonso-Zarza, A. M., & Wright, V. P. (2010). Chapter 5 calcretes. In *Developments in sedimentology* (Vol. 61, pp. 225–267). Elsevier. https://doi.org/10.1016/S0070-4571(09)06105-6

Arakel, A. V. (1986). Evolution of calcrete in palaeodrainages of the Lake napperby area, central Australia. *Palaeogeography, Palaeoclimatology, Palaeoecology*, *54*(1–4), 283–303. https://doi.org/10.1016/0031-0182(86)90129-X

Bachman, G. O., & Machette, M. N. (1977). Calcic soils and calcretes in the Southwestern United States. *US Geological Survey*.

Batianoff, G., & Singh, S. (2001). Central Queensland serpentine landforms, plant ecology and endemism. *South African Journal of Science*, *97*(11), 495–500.

Bishop, J. L., Dobrea, E. Z. N., McKeown, N. K., Parente, M., Ehlmann, B. L., Michalski, J. R., et al. (2008). Phyllosilicate diversity and past aqueous activity revealed at mawrth vallis, Mars. *Science*, *321*(5890), 830–833. https://doi.org/10.1126/science.1159699

Bohor, B. F., & Hughes, R. E. (1971). Scanning electron microscopy of clays and clay minerals. *Clays and Clay Minerals*, *19*(1), 49–54. https://doi.org/10.1346/CCMN.1971.0190105

Braithwaite, & Zedef (1996). Hydromagnesite stromatolites and sediments in an alkaline Lake, salda golu, Turkey. *SEPM Journal of Sedimentary Research*, *66*(5), 991–1002. https://doi.org/10.1306/D426845F-2B26-11D7-8648000102C1865D

Brewer, R., & Sleeman, J. R. (1964). Glaebules: Their definition, classification and interpretation. *Journal of Soil Science*, *15*(1), 66–78. https://doi.org/10.1111/j.1365-2389.1964.tb00245.x

Brossier, J., Altieri, F., De Sanctis, M. C., Frigeri, A., Ferrari, M., De Angelis, S., et al. (2022). Constraining the spectral behavior of the clay-bearing outcrops in Oxia planum, the landing site for ExoMars "Rosalind Franklin" rover. *Icarus*, *386*, 115114. https://doi.org/10.1016/j.icarus.2022.115114

Broz, A. P., Horgan, B., Kalucha, H., Johnson, J. R., Royer, C., Dehouck, E., et al. (2024). Diagenetic history and biosignature preservation potential of fine-grained rocks at hogwallow flats, jezero crater, Mars. *Journal of Geophysical Research: Planets*, *129*(11), e2024JE008520. https://doi.org/10.1029/2024JE008520

Bruce, M. C., & Niu, Y. (2000). Evidence for Palaeozoic magmatism recorded in the late Neoproterozoic Marlborough ophiolite, new England fold belt, central Queensland. *Australian Journal of Earth Sciences*, *47*(6), 1065–1076. https://doi.org/10.1046/j.1440-0952.2000.00834.x

Bultel, B., Viennet, J., Poulet, F., Carter, J., & Werner, S. C. (2019). Detection of carbonates in Martian weathering profiles. *Journal of Geophysical Research: Planets*, *124*(4), 989–1007. https://doi.org/10.1029/2018JE005845

Cama, J., & Ganor, J. (2015). Dissolution kinetics of clay minerals. In *Developments in clay science* (Vol. 6, pp. 101–153). Elsevier. https://doi.org/10.1016/B978-0-08-100027-4.00004-8

Cardarelli, E. L., Árting, U., Paige, D. A., Hamran, S.-E., Russell, P., Andersson, F., et al. (2026). Ground penetrating radar observations of ancient large-scale deltaic structures in jezero crater, Mars. *Science Advances*, *12*(12), eadz6095. https://doi.org/10.1126/sciadv.adz6095

Carroll, D., & Starkey, H. C. (1958). Effect of sea-water on clay minerals. *Clays and Clay Minerals*, *7*, 80–101. https://doi.org/10.1346/CCMN.1958.0070103

Catling, D. C. (1999). A chemical model for evaporites on early Mars: Possible sedimentary tracers of the early climate and implications for exploration. *Journal of Geophysical Research*, *104*(E7), 16453–16469. https://doi.org/10.1029/1998JE001020

Clavé, E., Benzerara, K., Meslin, P.-Y., Forni, O., Royer, C., Mandon, L., et al. (2023). Carbonate detection with SuperCam in igneous rocks on the floor of jezero crater, Mars. *Journal of Geophysical Research: Planets*, *128*(6), e2022JE007463. https://doi.org/10.1029/2022JE007463

Clavé, E., Beyssac, O., Beck, P., Royer, C., Mandon, L., Mangold, N., et al. (2026). In situ carbonation of sedimentary and igneous rocks of ultramafic composition in jezero crater, Mars. *Journal of Geophysical Research: Planets*, *131*(4), e2025JE009107. https://doi.org/10.1029/2025JE009107

Corpolongo, A., Jakubek, R. S., Burton, A. S., Brown, A. J., Yanchilina, A., Czaja, A. D., et al. (2023). SHERLOC raman mineral class detections of the Mars 2020 crater floor campaign. *Journal of Geophysical Research: Planets*, *128*(3), e2022JE007455. https://doi.org/10.1029/2022JE007455

Corrigan, C. M., & Harvey, R. P. (2004). Multi-generational carbonate assemblages in Martian meteorite allan hills 84001: Implications for nucleation, growth, and alteration. *Meteoritics and Planetary Science*, *39*(1), 17–30. https://doi.org/10.1111/j.1945-5100.2004.tb00047.x

Deelman, J. C., & Eindhoven. (1999). Low-temperature nucleation of magnesite and dolomite. *Neues Jahrbuch Fur Mineralogie-Monatshefte*, 289–302.

Diaz-Hernandez, J. L., Sánchez-Navas, A., Delgado, A., Yepes, J., & Garcia-Casco, A. (2018). Textural and isotopic evidence for Ca-Mg carbonate pedogenesis. *Geochimica et Cosmochimica Acta*, *222*, 485–507. https://doi.org/10.1016/j.gca.2017.11.006

Dos Anjos, A. P. A., Sifeddine, A., Sanders, C. J., & Patchineelam, S. R. (2011). Synthesis of magnesite at low temperature. *Carbonates and Evaporites*, *26*(3), 213–215. https://doi.org/10.1007/s13146-011-0063-4

Ehlmann, B. L., Mustard, J. F., Murchie, S. L., Poulet, F., Bishop, J. L., Brown, A. J., et al. (2008). Orbital identification of carbonate-bearing rocks on Mars. *Science*, *322*(5909), 1828–1832. https://doi.org/10.1126/science.1164759

Eren, M., Kaplan, M. Y., Kadir, S., & Kapur, S. (2018). Biogenic (β-fabric) features in the hard laminated crusts of the Mersin and Adana regions, southern Turkey and the role of soil organisms in the formation of the calcrete profiles. *Catena*, *168*, 34–46. https://doi.org/10.1016/j.catena.2017.12.021

Evans, P. R., & Roberts, J. (1979). Evolution of central eastern Australia during the late Palaeozoic and early Mesozoic. *Journal of the Geological Society of Australia*, *26*(7–8), 325–340. https://doi.org/10.1080/00167617908729100

Falk, E. S., & Kelemen, P. B. (2015). Geochemistry and petrology of listvenite in the Samail ophiolite, Sultanate of Oman: Complete carbonation of peridotite during ophiolite emplacement. *Geochimica et Cosmochimica Acta*, *160*, 70–90. https://doi.org/10.1016/j.gca.2015.03.014

Farley, K., & Stack, K. (2024). Mars 2020 Initial reports (Vol. *4*). https://doi.org/10.17189/MZX3-K371

Fischel, M. H. H., Clarke, C. E., & Sparks, D. L. (2023). Synchrotron resolved microscale and bulk mineralogy in manganese-rich soils and associated pedogenic concretions. *Geoderma*, *430*, 116305. https://doi.org/10.1016/j.geoderma.2022.116305

Forster, B., & Baker, D. (1997). Characterisation of the serpentinite soils of central Queensland, Australia. In T. T Jaffré, R. D. Reeves, & T. Becquer (Eds.), *Écologie Des Milieux Sur Roches Ultramafiques et Sur Sols Métallifères. Documents Scientifiques et Techniques No. III/2'* (pp. 27–37).

Foster, L., Eggleton, R. A., & Roach, I. (2002). The Marlborough nickel laterite deposits. In *Presented at the regolith and landscapes in eastern Australia conference, CRC LEME* (Vol. 1, pp. 33–36). Citeseer.

Freeze, R. A. (1974). Streamflow generation. *Reviews of Geophysics*, *12*(4), 627–647. https://doi.org/10.1029/RG012i004p00627

García Del Real, P., & Vishal, V. (2016). Mineral carbonation in ultramafic and basaltic rocks. In V. Vishal & T. N. Singh (Eds.), *Geologic carbon sequestration* (pp. 213–229). Springer International Publishing. https://doi.org/10.1007/978-3-319-27019-7_11

Gaudin, A., Dehouck, E., & Mangold, N. (2011). Evidence for weathering on early Mars from a comparison with terrestrial weathering profiles. *Icarus*, *216*(1), 257–268. https://doi.org/10.1016/j.icarus.2011.09.004

Gile, L. H., Peterson, F. F., & Grossman, R. B. (1966). Morphological and genetic sequences of carbonate accumulation in desert soils. *Soil Science*, *101*(5), 347–360. https://doi.org/10.1097/00010694-196605000-00001

Goudie, A. S. (1983). Calcrete (pp. 93–131).

Halevy, I., Fischer, W. W., & Eiler, J. M. (2011). Carbonates in the Martian meteorite allan Hills 84001 formed at 18 ± 4°C in a near-surface aqueous environment. *Proceedings of the National Academy of Sciences*, *108*(41), 16895–16899. https://doi.org/10.1073/pnas.1109444108

Hobbs, F. W. C., & Xu, H. (2020). Magnesite formation through temperature and pH cycling as a proxy for lagoon and playa paleoenvironments. *Geochimica et Cosmochimica Acta*, *269*, 101–116. https://doi.org/10.1016/j.gca.2019.10.014

Horgan, B. H. N., Anderson, R. B., Dromart, G., Amador, E. S., & Rice, M. S. (2020). The mineral diversity of Jezero crater: Evidence for possible lacustrine carbonates on Mars. *Icarus*, *339*, 113526. https://doi.org/10.1016/j.icarus.2019.113526

Jones, A. J., Gupta, S., Barnes, R., Horgan, B. H. N., Williford, K. H., Paar, G., et al. (2026). Stratigraphy of carbonate-bearing rocks at the margin of jezero crater, Mars: Evidence for shoreline processes? *Journal of Geophysical Research: Planets*, *131*(1), e2025JE009111. https://doi.org/10.1029/2025JE009111

Kadir, S., Eren, M., Külah, T., Erkoyun, H., Huggett, J., & Önalgil, N. (2018). Genesis of palygorskite and calcretes in Pliocene Eskişehir basin, west central Anatolia, Turkey. *Catena*, *168*, 62–78. https://doi.org/10.1016/j.catena.2017.09.027

Kalucha, H., Broz, A., Randazzo, N., Aramendia, J., Madariaga, J. M., Garczynski, B., et al. (2024). Probable concretions observed in the shenandoah formation of jezero crater, Mars and comparison with terrestrial analogs. *Journal of Geophysical Research: Planets*, *129*(8), e2023JE008138. https://doi.org/10.1029/2023JE008138

Kaplan, M., Eren, M., Kadir, S., Kapur, S., & Huggett, J. (2014). A microscopic approach to the pedogenic formation of palygorskite associated with Quaternary calcretes of the Adana area, southern Turkey. *Turkish Journal of Earth Sciences*, *23*, 559–574. https://doi.org/10.3906/yer-1401-3

Khalidy, R., Arnaud, E., & Santos, R. M. (2022). Natural and human-induced factors on the accumulation and migration of pedogenic carbonate in soil: A review. *Land*, *11*(9), 1448. https://doi.org/10.3390/land11091448

Khitrov, N. B. (2016). The genesis of vertisols with gilgai microtopography: A review. *Eurasian Soil Science*, *49*(5), 489–497. https://doi.org/10.1134/S1064229316050070

Kite, E. S., Tutolo, B. M., Turner, M. L., Franz, H. B., Burtt, D. G., Bristow, T. F., et al. (2025). Carbonate formation and fluctuating habitability on Mars. *Nature*, *643*(8070), 60–66. https://doi.org/10.1038/s41586-025-09161-1

Klingaman, N. P. (2012). Rainfall in Queensland: Part I: A literature survey of key rainfall drivers in Queensland Australia: Rainfall variability and change. *Department of Environmental and Resource Management*.

Kovda, I. (2020). Vertisols: Extreme features and extreme environment. *Geoderma Regional*, *22*, e00312. https://doi.org/10.1016/j.geodrs.2020.e00312

Kuzyakov, Y., & Blagodatskaya, E. (2015). Microbial hotspots and hot moments in soil: Concept and review. *Soil Biology and Biochemistry*, *83*, 184–199. https://doi.org/10.1016/j.soilbio.2015.01.025

Leon, E., Vargas, R., Bullock, S., Lopez, E., Panosso, A. R., & La Scala, N. (2014). Hot spots, hot moments, and spatio-temporal controls on soil CO_2 efflux in a water-limited ecosystem. *Soil Biology and Biochemistry*, *77*, 12–21. https://doi.org/10.1016/j.soilbio.2014.05.029

Leshin, L. A., Mahaffy, P. R., Webster, C. R., Cabane, M., Coll, P., Conrad, P. G., et al. (2013). Volatile, isotope, and organic analysis of Martian fines with the Mars curiosity rover. *Science*, *341*(6153), 1238937. https://doi.org/10.1126/science.1238937

Lin, H. (2011). Three principles of soil change and pedogenesis in time and space. *Soil Science Society of America Journal*, *75*(6), 2049–2070. https://doi.org/10.2136/sssaj2011.0130

Liu, Y., Treiman, A., Schmidt, M., Tice, M., Jones, M., VanBommel, S., et al. (2026). Discovery of ancient granitic components outside jezero crater, Mars. *57th Lunar and Planetary Science Conference*, *3160*, 1322.

Loizeau, D., Mangold, N., Poulet, F., Bibring, J.-P., Bishop, J. L., Michalski, J., & Quantin, C. (2015). History of the clay-rich unit at mawrth vallis, Mars: High-resolution mapping of a candidate landing site: HIGH-RESOLUTION mapping at mawrth vallis. *Journal of Geophysical Research: Planets*, *120*(11), 1820–1846. https://doi.org/10.1002/2015JE004894

Lumsden. (1988). Characteristics of deep-marine dolomite. *SEPM Journal of Sedimentary Research*, *58*. https://doi.org/10.1306/212F8EEF-2B24-11D7-8648000102C1865D

Mandon, L., Parkes Bowen, A., Quantin-Nataf, C., Bridges, J. C., Carter, J., Pan, L., et al. (2021). Morphological and spectral diversity of the clay-bearing unit at the ExoMars landing site Oxia planum. *Astrobiology*, *21*(4), 464–480. https://doi.org/10.1089/ast.2020.2292

Mandon, L., Quantin-Nataf, C., Thollot, P., Mangold, N., Lozac'h, L., Dromart, G., et al. (2020). Refining the age, emplacement and alteration scenarios of the olivine-rich unit in the nili fossae region, Mars. *Icarus*, *336*, 113436. https://doi.org/10.1016/j.icarus.2019.113436

Mavromatis, V., Power, I. M., Harrison, A. L., Beinlich, A., Dipple, G. M., & Bénézeth, P. (2021). Mechanisms controlling the Mg isotope composition of hydromagnesite-magnesite playas near Atlin, British Columbia, Canada. *Chemical Geology*, *579*, 120325. https://doi.org/10.1016/j.chemgeo.2021.120325

McClain, M. E., Boyer, E. W., Dent, C. L., Gergel, S. E., Grimm, N. B., Groffman, P. M., et al. (2003). Biogeochemical hot spots and hot moments at the interface of terrestrial and aquatic ecosystems. *Ecosystems*, *6*(4), 301–312. https://doi.org/10.1007/s10021-003-0161-9

McLaren, S., & Gardner, R. (2004). Late Quaternary vadose carbonate diagenesis in coastal and desert dune and beach sands: Is there a palaeoclimatic signal? *Earth Surface Processes and Landforms*, *29*(12), 1441–1458. https://doi.org/10.1002/esp.1132

McNeil, V. H., & Raymond, M. A. A. (2013). Mapping regional groundwater chemistry zones in the Fitzroy basin, using statistical and conceptual methods. *Proceedings of the Royal Society of Queensland*, *118*, 37–61. https://doi.org/10.5962/p.357778

McQueen, K. G., Hill, S. M., & Foster, K. A. (1999). The nature and distribution of regolith carbonate accumulations in southeastern Australia and their potential as a sampling medium in geochemical exploration. *Journal of Geochemical Exploration*, *67*(1–3), 67–82. https://doi.org/10.1016/S0375-6742(99)00071-0

Michalski, J. R., Cuadros, J., Niles, P. B., Parnell, J., Deanne Rogers, A., & Wright, S. P. (2013). Groundwater activity on Mars and implications for a deep biosphere. *Nature Geoscience*, *6*(2), 133–138. https://doi.org/10.1038/ngeo1706

Milburn, D., & Wilcock, S. (1998). Kunwarara magnesite deposit. *Geol Aust Papua New Guinean Min Depos, Australasian Inst Min and Metall Monogr*, *22*, 815–818.

Miller, W. L., Kishné, A. S., & Morgan, C. L. S. (2010). Vertisol morphology, classification, and seasonal cracking patterns in the Texas Gulf Coast prairie. *Soil Survey Horizons*, *51*(1), 10–16. https://doi.org/10.2136/sh2010.1.0010

Milnes, A., & Hutton, J. T. (1983). Calcretes in Australia - A review (pp. 119–162).

Mittlefehldt, D. W. (1994). ALH84001, a cumulate orthopyroxenite member of the martian meteorite clan. *Meteoritics*, *29*(2), 214–221. https://doi.org/10.1111/j.1945-5100.1994.tb00673.x

Montes-Hernandez, G., Renard, F., Auzende, A.-L., & Findling, N. (2020). Amorphous calcium–magnesium carbonate (ACMC) accelerates dolomitization at room temperature under abiotic conditions. *Crystal Growth and Design*, *20*(3), 1434–1441. https://doi.org/10.1021/acs.cgd.9b01005

Morris, R. V., Ruff, S. W., Gellert, R., Ming, D. W., Arvidson, R. E., Clark, B. C., et al. (2010). Identification of carbonate-rich outcrops on Mars by the spirit rover. *Science*, *329*(5990), 421–424. https://doi.org/10.1126/science.1189667

Murray, C. G. (2007). Devonian supra-subduction zone setting for the princhester and northumberland serpentinites: Implications for the tectonic evolution of the northern new England Orogen. *Australian Journal of Earth Sciences*, *54*(7), 899–925. https://doi.org/10.1080/08120090701392747

Nash, D. J., & McLaren, S. J. (2003). Kalahari valley calcretes: Their nature, origins, and environmental significance. *Quaternary International*, *111*(1), 3–22. https://doi.org/10.1016/S1040-6182(03)00011-9

Ning, M., Luo, J., Liang, Z., Huang, P., Xing, C., & Shen, B. (2025). Pedogenic carbonates in deep time: Characteristics, geological significance, and co-evolution with plant terrestrialization. *Earth-Science Reviews*, *271*, 105314. https://doi.org/10.1016/j.earscirev.2025.105314

Oskierski, H. C., Bailey, J. G., Kennedy, E. M., Jacobsen, G., Ashley, P. M., & Dlugogorski, B. Z. (2013). Formation of weathering-derived magnesite deposits in the New England Orogen, New South Wales, Australia: Implications from mineralogy, geochemistry and genesis of the Attunga magnesite deposit. *Mineralium Deposita*, *48*(4), 525–541. https://doi.org/10.1007/s00126-012-0440-5

Oskierski, H. C., Beinlich, A., Mavromatis, V., Altarawneh, M., & Dlugogorski, B. Z. (2019). Mg isotope fractionation during continental weathering and low temperature carbonation of ultramafic rocks. *Geochimica et Cosmochimica Acta*, *262*, 60–77. https://doi.org/10.1016/j.gca.2019.07.019

Peralta, A. L., Ludmer, S., Matthews, J. W., & Kent, A. D. (2014). Bacterial community response to changes in soil redox potential along a moisture gradient in restored wetlands. *Ecological Engineering*, *73*, 246–253. https://doi.org/10.1016/j.ecoleng.2014.09.047

Pett-Ridge, J., & Firestone, M. K. (2005). Redox fluctuation structures microbial communities in a wet tropical soil. *Applied and Environmental Microbiology*, *71*(11), 6998–7007. https://doi.org/10.1128/AEM.71.11.6998-7007.2005

Phua, Y. Y., Ehlmann, B. L., Siljeström, S., Czaja, A. D., Beck, P., Connell, S., et al. (2024). Characterizing hydrated sulfates and altered phases in jezero crater fan and floor geologic units with SHERLOC on Mars 2020. *Journal of Geophysical Research: Planets*, *129*(7), e2023JE008251. https://doi.org/10.1029/2023JE008251

Pohl, W. (1989). Comparative geology of magnesite deposits and occurrences. *Monograph Series on Mineral Deposits*, *28*, 1–13.

Power, I. M., Harrison, A. L., Dipple, G. M., Wilson, S., Barker, S. L. L., & Fallon, S. J. (2019). Magnesite formation in playa environments near atlin, British Columbia, Canada. *Geochimica et Cosmochimica Acta*, *255*, 1–24. https://doi.org/10.1016/j.gca.2019.04.008

Power, I. M., Kenward, P. A., Dipple, G. M., & Raudsepp, M. (2017). Room temperature magnesite precipitation. *Crystal Growth and Design*, *17*(11), 5652–5659. https://doi.org/10.1021/acs.cgd.7b00311

Raudsepp, M. J., Wilson, S., Zeyen, N., Arizaleta, M. L., & Power, I. M. (2024). Magnesite everywhere: Formation of carbonates in the alkaline Lakes and playas of the cariboo Plateau, British Columbia, Canada. *Chemical Geology*, *648*, 121951. https://doi.org/10.1016/j.chemgeo.2024.121951

Rezanezhad, F., Couture, R.-M., Kovac, R., O'Connell, D., & Van Cappellen, P. (2014). Water table fluctuations and soil biogeochemistry: An experimental approach using an automated soil column system. *Journal of Hydrology*, *509*, 245–256. https://doi.org/10.1016/j.jhydrol.2013.11.036

Riechelmann, S., Mavromatis, V., Buhl, D., Dietzel, M., & Immenhauser, A. (2020). Controls on formation and alteration of early diagenetic dolomite: A multi-proxy δ44/40Ca, δ26Mg, δ18O and δ13C approach. *Geochimica et Cosmochimica Acta*, *283*, 167–183. https://doi.org/10.1016/j.gca.2020.06.010

Rubol, S., Silver, W. L., & Bellin, A. (2012). Hydrologic control on redox and nitrogen dynamics in a peatland soil. *Science of The Total Environment*, *432*, 37–46. https://doi.org/10.1016/j.scitotenv.2012.05.073

Scheller, E. L., Razzell Hollis, J., Cardarelli, E. L., Steele, A., Beegle, L. W., Bhartia, R., et al. (2022). Aqueous alteration processes in jezero crater, Mars—Implications for organic geochemistry. *Science*, *378*(6624), 1105–1110. https://doi.org/10.1126/science.abo5204

Scheller, E. L., Swindle, C., Grotzinger, J., Barnhart, H., Bhattacharjee, S., Ehlmann, B. L., et al. (2021). Formation of magnesium carbonates on Earth and implications for Mars. *Journal of Geophysical Research: Planets*, *126*(7), e2021JE006828. https://doi.org/10.1029/2021JE006828

Scott, E. R. D., Krot, A. N., & Yamaguchi, A. (1998). Carbonates in fractures of Martian meteorite allan hills 84001: Petrologic evidence for impact origin. *Meteoritics and Planetary Science*, *33*(4), 709–719. https://doi.org/10.1111/j.1945-5100.1998.tb01677.x

Sheppard, R. Y., Loizeau, D., Fraeman, A. A., Rampe, E. B., Pilorget, C., & Bibring, J.-P. (2025). Mg-sulfate can spectrally obscure siderite: Implications for martian surface carbonates. *Frontiers in Astronomy and Space Sciences*, *12*, 1549242. https://doi.org/10.3389/fspas.2025.1549242

Shumway, A. O., Kizovski, T. V., Catling, D. C., VanBommel, S. J., Jones, M. W. M., Orenstein, B. J., et al. (2025). Mineralogically diverse and salt-rich regolith in jezero crater characterized using X-ray spectroscopy. *Journal of Geophysical Research: Planets*, *130*(10), e2024JE008912. https://doi.org/10.1029/2024JE008912

Smith, A. P., Bond-Lamberty, B., Benscoter, B. W., Tfaily, M. M., Hinkle, C. R., Liu, C., & Bailey, V. L. (2017). Shifts in pore connectivity from precipitation versus groundwater rewetting increases soil carbon loss after drought. *Nature Communications*, *8*(1), 1335. https://doi.org/10.1038/s41467-017-01320-x

Spötl, C., & Burns, S. J. (1994). Magnesite diagenesis in redbeds: A case study from the Permian of the northern calcareous Alps (tyrol, Austria). *Sedimentology*, *41*(3), 543–565. https://doi.org/10.1111/j.1365-3091.1994.tb02010.x

Steele, A., Benning, L. G., Wirth, R., Schreiber, A., Araki, T., McCubbin, F. M., et al. (2022). Organic synthesis associated with serpentinization and carbonation on early Mars. *Science*, *375*(6577), 172–177. https://doi.org/10.1126/science.abg7905

Stegen, J., Burgin, A. J., Busch, M. H., Fisher, J. B., Ladau, J., Abrahamson, J., et al. (2025). Reviews and syntheses: Variable inundation across Earth's terrestrial ecosystems. *Biogeosciences*, *22*(4), 995–1034. https://doi.org/10.5194/bg-22-995-2025

Stern, J. C., Sutter, B., Archer, P. D., Eigenbrode, J. L., McAdam, A. C., Franz, H. B., et al. (2018). Major volatiles evolved from Eolian materials in gale crater. *Geophysical Research Letters*, *45*(19). https://doi.org/10.1029/2018GL079059

Sutter, B., Boynton, W. V., Ming, D. W., Niles, P. B., Morris, R. V., Golden, D. C., et al. (2012). The detection of carbonate in the Martian soil at the phoenix landing site: A laboratory investigation and comparison with the thermal and evolved Gas Analyzer (TEGA) data. *Icarus*, *218*(1), 290–296. https://doi.org/10.1016/j.icarus.2011.12.002

Swindle, C., Vasconcelos, P., Dalleska, N., Cardarelli, E., Bhattacharjee, S., Dimarco, Z., et al. (2025). Trace element compositions and redox shifts preserved in magnesites, sediments and soils from the kunwarara magnesite mine. *Applied Geochemistry*, *191*, 106494. https://doi.org/10.1016/j.apgeochem.2025.106494

Swindle, C., Vasconcelos, P., Dimarco, Z., Dalleska, N., Nguyen, A., Cardarelli, E., et al. (2025). Elemental signatures of metamorphic, diagenetic, and pedogenic magnesites from central Queensland, Australia. *Chemical Geology*, *695*, 123068. https://doi.org/10.1016/j.chemgeo.2025.123068

Tarnas, J. D., Stack, K. M., Parente, M., Koeppel, A. H. D., Mustard, J. F., Moore, K. R., et al. (2021). Characteristics, origins, and biosignature preservation potential of carbonate-bearing rocks within and outside of jezero crater. *Journal of Geophysical Research: Planets*, *126*(11), e2021JE006898. https://doi.org/10.1029/2021JE006898

Treiman, A. H. (1995). A petrographic history of martian meteorite ALH84001: Two shocks and an ancient age. *Meteoritics*, *30*(3), 294–302. https://doi.org/10.1111/j.1945-5100.1995.tb01127.x

Tutolo, B. M., Hausrath, E. M., Kite, E. S., Rampe, E. B., Bristow, T. F., Downs, R. T., et al. (2025). Carbonates identified by the Curiosity rover indicate a carbon cycle operated on ancient Mars. *Science*, *388*(6744), 292–297. https://doi.org/10.1126/science.ado9966

Valdespino-Castillo, P. M., Águila, B., Torres-Huesca, J., Centeno, C. M., Martínez-Díaz, J., Reyes-Salas, M., et al. (2022). Microbialites: Diversity hotspots in the Mexican Plateau. In J. Alcocer (Ed.), *Lake Alchichica limnology* (pp. 375–390). Springer International Publishing. https://doi.org/10.1007/978-3-030-79096-7_22

Williford, K. H., Farley, K. A., Horgan, B. H. N., Garczynski, B., Treiman, A. H., Gupta, S., et al. (2025). Carbonated ultramafic igneous rocks in Jezero crater, Mars. *Science*, *391*(6787), eadu8264. https://doi.org/10.1126/science.adu8264

Williford, K. H., Farley, K. A., Horgan, B. H. N., Garczynski, B., Treiman, A. H., Gupta, S., et al. (2026). Carbonated ultramafic igneous rocks in Jezero crater, Mars. *Science*, *391*(6787), eadu8264. https://doi.org/10.1126/science.adu8264

Wright, V. P. (1982). Calcrete palaeosols from the Lower Carboniferous Llanelly Formation, South Wales. *Sedimentary Geology*, *33*(1), 1–33.

Wright, V. P. (2007). Calcrete. In D. J. Nash & S. J. McLaren (Eds.), *Geochemical sediments and landscapes* (1st ed., pp. 10–45). Wiley. https://doi.org/10.1002/9780470712917.ch2

Zamanian, K., Pustovoytov, K., & Kuzyakov, Y. (2016). Pedogenic carbonates: Forms and formation processes. *Earth-Science Reviews*, *157*, 1–17. https://doi.org/10.1016/j.earscirev.2016.03.003

Zeissink, H. E. (1969). The mineralogy and geochemistry of a nickeliferous laterite profile (Greenvale, Queensland, Australia). *Mineralium Deposita*, *4*(2). https://doi.org/10.1007/BF00208049

Zhang, Z., & Furman, A. (2021). Soil redox dynamics under dynamic hydrologic regimes - A review. *Science of The Total Environment*, *763*, 143026. https://doi.org/10.1016/j.scitotenv.2020.143026